RESEARCH REPORT

Functional implications of Ca$_v$2.3 R-type voltage-gated calcium channels in the murine auditory system – novel vistas from brainstem-evoked response audiometry

Andreas Lundt[1] | Julien Soós[1] | Robin Seidel[2] | Christina Henseler[1] | Ralf Müller[3] | Varun Raj Ginde[1] | Muhammad Imran Arshaad[1] | Dan Ehninger[4] | Jürgen Hescheler[5] | Agapios Sachinidis[5] | Karl Broich[2] | Carola Wormuth[1] | Anna Papazoglou[1] | Marco Weiergräber[1] (ID)

[1]Experimental Neuropsychopharmacology, Federal Institute for Drugs and Medical Devices (Bundesinstitut für Arzneimittel und Medizinprodukte, BfArM), Bonn, Germany

[2]Federal Institute for Drugs and Medical Devices (Bundesinstitut für Arzneimittel und Medizinprodukte, BfArM), Bonn, Germany

[3]Cognitive Neurophysiology, Department of Psychiatry and Psychotherapy and University Hospital Cologne, Faculty of Medicine, University of Cologne, Cologne, Germany

[4]Molecular and Cellular Cognition, German Center for Neurodegenerative Diseases, (Deutsches Zentrum für Neurodegenerative Erkrankungen, DZNE), Bonn, Germany

[5]Institute of Neurophysiology, Faculty of Medicine, University of Cologne, Cologne, Germany

Correspondence
Marco Weiergräber, Experimental Neuropsychopharmacology, Federal Institute for Drugs and Medical Devices (Bundesinstitut für Arzneimittel und Medizinprodukte, BfArM), Kurt-Georg-Kiesinger-Allee 3, 53175 Bonn, Germany.
Email: Marco.Weiergraeber@bfarm.de

Present addresses
Andreas Lundt, KBRwyle GmbH, Linder Höhe, 51147 Cologne, Germany.

Julien Soós, Institut für Pathophysiologie, Universitätsmedizin

Abstract

Voltage-gated Ca^{2+} channels (VGCCs) are considered to play a key role in auditory perception and information processing within the murine inner ear and brainstem. In the past, Ca$_v$1.3 L-type VGCCs gathered most attention as their ablation causes congenital deafness. However, isolated patch-clamp investigation and localization studies repetitively suggested that Ca$_v$2.3 R-type VGCCs are also expressed in the cochlea and further components of the ascending auditory tract, pointing to a potential functional role of Ca$_v$2.3 in hearing physiology. Thus, we performed auditory profiling of Ca$_v$2.3$^{+/+}$ controls, heterozygous Ca$_v$2.3$^{+/-}$ mice and Ca$_v$2.3 null mutants (Ca$_v$2.3$^{-/-}$) using brainstem-evoked response audiometry. Interestingly,

Abbreviations: (q)PCR, quantitative polymerase chain reaction; ABR, auditory brainstem response; AChR, acetylcholine receptor; AED, antiepileptic drug; AEP, auditory evoked potential; ARHL, age-related hearing loss; AVCN, anteroventral cochlear nucleus; BERA, brainstem-evoked response audiometry; BK, big conductance Ca^{2+}-activated K$^+$ channel; CNRQ, calibrated normalized relative quantities; CWT, continuous wavelet transform; DHP, dihydropyridine; FFT, fast Fourier transformation; HC, hair cell; HVA, high voltage-activated; i.p., intraperitoneal; IC, inferior colliculus; IHC, inner hair cell; ILD, interaural level detection; IWI, interwave interval; LL, lateral lemniscus; LSO, lateral superior olive; LVA, low voltage-activated; MNTB, medial nucleus of the trapezoid body; MVA, mid voltage-activated; NIHL, noise-induced hearing loss; OHC, outer hair cell; RT, reverse transcription; RTN, reticular thalamic nucleus; SD, standard deviation; SEM, standard error of the mean; SGN, spiral ganglion neuron; SK, small conductance Ca^{2+}-activated K$^+$ channel; SNR, signal-to-noise ratio; SOC, superior olivary complex; SPL, sound pressure level; SPON, superior paraolivary nucleus; TTX, tetrodotoxin; TWs, time windows; VGCC, voltage-gated Ca^{2+} channel.

Edited by Marco Capogna.

Greifswald, Martin-Lutherstr. 6, 17489
Greifswald, Germany

Varun Raj Ginde, Animal
Sleep Lab, Hal U11, Neurology
Department, Universitätspital Zürich,
Frauenklinikstrasse 26, 8091 Zürich,
Germany

Carola Wormuth, Thescon GmbH,
Gottfriedweg 22, 48653 Coesfeld, Germany

click-evoked auditory brainstem responses (ABRs) revealed increased hearing thresholds in $Ca_v2.3^{+/-}$ mice from both genders, whereas no alterations were observed in $Ca_v2.3^{-/-}$ mice. Similar observations were made for tone burst-related ABRs in both genders. However, $Ca_v2.3$ ablation seemed to prevent mutant mice from total hearing loss particularly in the higher frequency range (36–42 kHz). Amplitude growth function analysis revealed, i.a., significant reduction in ABR wave W_I and W_{III} amplitude in mutant animals. In addition, alterations in W_I-W_{IV} interwave interval were observed in female $Ca_v2.3^{+/-}$ mice whereas absolute latencies remained unchanged. In summary, our results demonstrate that $Ca_v2.3$ VGCCs are mandatory for physiological auditory information processing in the ascending auditory tract.

KEYWORDS

auditory brainstem response, calcium channel, hair cells, hearing loss, R-type

1 | INTRODUCTION

Voltage-gated Ca^{2+} channels (VGCCs) are of central relevance in mediating Ca^{2+} influx into living cells. Based on electrophysiological and pharmacological properties, VGCCs are segregated into high voltage-activated (HVA) $Ca_v1.1$–1.4 L-type, HVA $Ca_v2.1$–2.3 Non-L-type and low voltage-activated (LVA) $Ca_v3.1$–3.3 T-type Ca^{2+} channels (Catterall, Perez-Reyes, Snutch, & Striessnig, 2005; Soong et al., 1993; Williams et al., 1994). Some Ca_v channels were reported to be expressed and to have physiological relevance within the inner ear, for example, inner and outer hair cells (IHCs and OHCs, respectively), and the brainstem, for example, the spiral ganglion (SGN), the cochlear nucleus, the trapezoid body, the superior olivary complex (SOC) and further ascending structures (Joiner & Lee, 2015; Pangrsic, Singer, & Koschak, 2018). Two important VGCC entities are $Ca_v1.3$ L-type and $Ca_v2.3$ R-type Ca^{2+} channels, both of which expressed in the inner ear and auditory tract (Fell et al., 2016; Layton, Robertson, Everett, Mulders, & Yates, 2005; Pangrsic et al., 2018; Picher et al., 2017; Waka, Knipper, & Engel, 2003). $Ca_v2.3$ knockout mice exhibit a complex phenotype, for example, altered pancreatic beta cell function and glucose tolerance (Pereverzev et al., 2002; Yang & Berggren, 2005), cardiac arrhythmia and altered autonomic function (Galetin et al., 2013; Lu et al., 2004; Weiergraber et al., 2005), reduced seizure susceptibility (Kuzmiski, Barr, Zamponi, & MacVicar, 2005; Tai, Kuzmiski, & MacVicar, 2006; Weiergraber, Henry, et al., 2006a; Weiergraber, Henry, Radhakrishnan, Hescheler, & Schneider, 2007; Weiergraber, Kamp, Radhakrishnan, Hescheler, & Schneider, 2006b; Weiergraber, Stephani, & Kohling, 2010), dysregulation in hippocampal theta genesis (Muller et al., 2012) and impaired presynaptic long-term potentiation (LTP) (Dietrich et al., 2003), distorted circadian

rhythmicity and sleep (Siwek et al., 2014), altered myelinogenesis (Chen, Ren, Bing, & Hillman, 2000) and modified neuropathic pain perception (Matthews, Bee, Stephens, & Dickenson, 2007; Yokoyama et al., 2004). Notably, heterozygous $Ca_v2.3^{+/-}$ mice were hardly included in previous studies and no auditory analysis has been carried out so far.

Importantly, $Ca_v2.3$ VGCCs serve as key elements in regulating neuronal firing modes within the CNS. These include the tonic, intermediate and burst firing modes that regulate facultative neuronal oscillatory properties in specific neuronal populations (Bloodgood & Sabatini, 2007, 2009; Higley & Sabatini, 2008, 2012).

Within the VGCC family, complex alterations in auditory processing were first reported for $Ca_v1.3$ mutant mice. In 2000, Platzer et al. reported that ablation of the HVA $Ca_v1.3$ L-type VGCC causes deafness and degeneration of IHCs and OHCs in mice (Platzer et al., 2000). Later, hearing deficits were also detected in heterozygous $Ca_v1.3^{+/-}$ mice, manifested by an increase in threshold of low-frequency sounds (Dou et al., 2004). Interestingly, the balance performance in $Ca_v1.3^{-/-}$ mice was comparable to their wild-type littermates (Dou et al., 2004) pointing to a differential functional expression of this Ca^{2+} channel in the cochlea and vestibular system. Notably, $Ca_v1.3$ VGCC accounted for about 90% of Ca^{2+} influx into IHCs and studies in $Ca_v1.3^{-/-}$ mice suggested that the remaining current could be $Ca_v1.4$ dependent (Brandt, Striessnig, & Moser, 2003; Engel, Michna, Platzer, & Striessnig, 2002; Michna et al., 2003). Secondary compensatory mechanisms in mutant mice may contribute to this observation as well. Using both genetic disruption of cacna1d and acute pharmacological block of $Ca_v1.3$ VGCCs, Sheets, Kindt and Nicolson (2012) further demonstrated that Ca^{2+} influx via $Ca_v1.3$ Ca^{2+} channels fine-tunes synaptic ribbon size during hair-cell maturation and that $Ca_v1.3$ is essential for maintenance of the

active zone of HCs. As expected, $Ca_v1.3^{-/-}$ IHCs exhibited only marginal exocytosis, lacked early Ca^{2+}-dependent action potentials and exhibited a complex developmental failure (Brandt et al., 2003). Similar to the IHCs, VGCCs also seem to be mandatory for the maturation of OHCs as the latter degenerate in $Ca_v1.3^{-/-}$ mice shortly after the time point of normal physiological onset of hearing (Glueckert et al., 2003; Michna et al., 2003). Whereas $Ca_v1.3$ L-type Ca^{2+} channels have been in the focus of interest, the low resting potentials of OHCs and their slight depolarization upon sound stimuli suggest that LVA Ca^{2+} channels may also contribute to intracellular Ca^{2+} regulation (Inagaki, Ugawa, Yamamura, Murakami, & Shimada, 2008). L-type Ca^{2+} channels are likely to play a role in phasic neurotransmitter release (Dou et al., 2004), and the function of other VGCC entities may be obscured by their baseline activity and minimal contribution to Ca^{2+} influx in hair cells (HCs) (Moser & Beutner, 2000; Spassova, Eisen, Saunders, & Parsons, 2001). Indeed, Dou et al. (2004) early suggested that other VGCCs contribute to the remaining dihydropyridine (DHP)-insensitive Ca^{2+} current in HCs (Su, Jiang, Gu, & Yang, 1995; Platzer et al., 2000; Martini et al., 2000; Rodriguez-Contreras & Yamoah, 2001).

$Ca_v2.3$ VGCCs could serve as one of these candidates. From P2 to P10, $Ca_v2.3$ VGCCs seem to be expressed in the outer rather than the inner spiral bundle efferent endings and in medial efferent fibres. Astonishingly, $Ca_v2.3$ expression vanished around P14 but was observed later at P19 in the basal poles of the OHC membranes again (Waka et al., 2003). In addition, electrophysiological studies, in situ hybridization and RT-PCR also point to a functional expression of $Ca_v2.3$ in the ascending auditory tract (Parajuli et al., 2012; Soong et al., 1993; Williams et al., 1994). Functionally, $Ca_v2.3$ and $Ca_v1.3$ VGCCs share essential physiological properties. $Ca_v1.3$ was reported to be mid voltage-activated (MVA) to LVA instead of being a classical HVA Ca^{2+} channel (Koschak et al., 2001; Michna et al., 2003). The same holds true for $Ca_v2.3$, as demonstrated by recent studies showing that $Ca_v2.3$ Ca^{2+} channels can exhibit MVA to LVA properties depending on the presence or absence of divalent heavy metal ions in the brain (Shcheglovitov et al., 2012).

Additionally, low micromolar concentrations of DHPs cannot be used to reliably discriminate between L-type from Non-L-type HVA channels and $Ca_v2.3$ can clearly underlie a low DHP-sensitive Ca^{2+} current component (Lu et al., 2004; Stephens, Page, Burley, Berrow, & Dolphin, 1997; Weiergraber, Kamp, et al., 2006b). Considering that $Ca_v1.3$ and $Ca_v2.3$ VGCCs are coexpressed in many regions, it becomes obvious that both channels might functionally contribute to a low- to mid voltage-activated and low DHP-sensitive Ca^{2+} current component in the auditory tract (Perez-Reyes, 2003; Shcheglovitov et al., 2012; Weiergraber, Kamp, et al., 2006b).

Based on these findings, we performed auditory profiling of $Ca_v2.3^{+/-}$ and $Ca_v2.3^{-/-}$ mice using brainstem-evoked response audiometry. Our results demonstrate complex alterations in click and tone burst-related hearing thresholds and amplitude growth function in $Ca_v2.3^{+/-}$ and $Ca_v2.3^{-/-}$ mice with a potential gene dose-dependent effect. This is the first report of altered auditory information processing in $Ca_v2.3$ mutant animals.

2 | METHODS

2.1 | Experimental animals

$Ca_v2.3^{+/-}$ embryos (kindly provided by Richard J. Miller; Department of Neurobiology Pharmacology, and Physiology; The University of Chicago; Chicago) were re-derived with C57BL/6J mice and maintained with random intra-strain mating obtaining all genotypes (Wilson et al., 2000). The mutant line was originally generated by the use of homologous recombination in which the S4–S6 region of domain II was replaced with a neomycin/URA3 selection cassette. Removal of the pore-lining and its neighbouring transmembrane regions resulted in a null allele of Cacna1e with no detectable $Ca_v2.3$ transcript in Northern blot analysis and no detectable $Ca_v2.3$ protein in Western blot analysis in $Ca_v2.3$ knockouts (Wilson et al., 2000). The resultant $Ca_v2.3^{-/-}$ mice represent a constitutive knockout.

The study included in total 58 mice, 18 $Ca_v2.3^{+/+}$ mice (9 ♀, mean body weight: 25.4 g ± 0.6 g and 9 ♂, mean body weight: 32.7 g ± 1.8 g), 19 $Ca_v2.3^{+/-}$ mice (10 ♀, mean body weight: 25.4 g ± 1.4 g and 9 ♂, mean body weight: 31.6 g ± 1.1 g) and 21 $Ca_v2.3^{-/-}$ mice (11 ♀, mean body weight: 27.0 g ± 0.4 g and 10 ♂, mean body weight: 31.1 g ± 0.9 g). ABR recordings were performed with mice aged 140–142 days (~20 weeks).

All mice were housed in groups of 2–5 in clear Makrolon cages type II with ad libitum access to drinking water and standard food pellets. Using ventilated cabinets (Model 9AV125PYN, Tecniplast, Germany; UniProtect, Zoonlab, Germany) as a noise-protected environment, mice were maintained at a temperature of 21 ± 2°C, 50%–60% relative humidity, and on a conventional 12-hr light/dark cycle with a light onset at 5:00 a.m. Prior to experimentation, the animals were strictly adapted to this circadian pattern for 14 days (Lundt, Seidel, et al., 2019; Lundt, Soos, et al., 2019).

All animal experimentation was carried out according to the guidelines of the German Council on Animal Care, and all protocols were approved by the local institutional and national committee on animal care (LANUV). The authors further certify that all animal experimentation was carried out in accordance with the National Institute of Health Guide for the Care and Use of Laboratory Animals (NIH Publications No. 80–23) revised 1996 or the UK Animals (Scientific Procedures) Act 1986 and associated guidelines, or the European Communities Council Directive of 24 November

1986 (86/609/ EEC) and of 22 September 2010 (2010/63/ EU) (Lundt, Seidel, et al., 2019; Lundt, Soos, et al., 2019). Specific effort was made to minimize the number of animals used and their suffering (3R strategy).

2.2 | Genotyping

$Ca_v2.3$ mutant mice were genotyped by PCR based on the protocol of the KAPA Mouse genotyping kit (Sigma-Aldrich, Germany). The following primers were used: WT forward 5′-GGC TGC TCT CCC AGT ATA CT-3′; WT reverse/KO reverse 5′-CAG GAA GCA TCA CTG CTT AG-3′; KO forward 5′-ATT GCA GTG AGC CAA GAT TGT GCC-3′. PCR was carried out using the C1000 thermal cycler (Bio-Rad) with an initial denaturation (95°C–1 min) followed by 35 cycles (each cycle containing the following steps: denaturation 95°C–15 s, annealing 59°C–15 s, extension 72°C–1 min) and final extension (72°C–10 min). Subsequently, PCR products were separated via agarose gel electrophoresis and detected by ChemiDoc Touch (Bio-Rad) (Figure 1a).

2.3 | Western blot

For microsome preparation, mice were decapitated, and the extirpated brains were placed on ice. The cortex of one $Ca_v2.3^{+/+}$, $Ca_v2.3^{+/-}$ and $Ca_v2.3^{-/-}$ mouse was dissected and
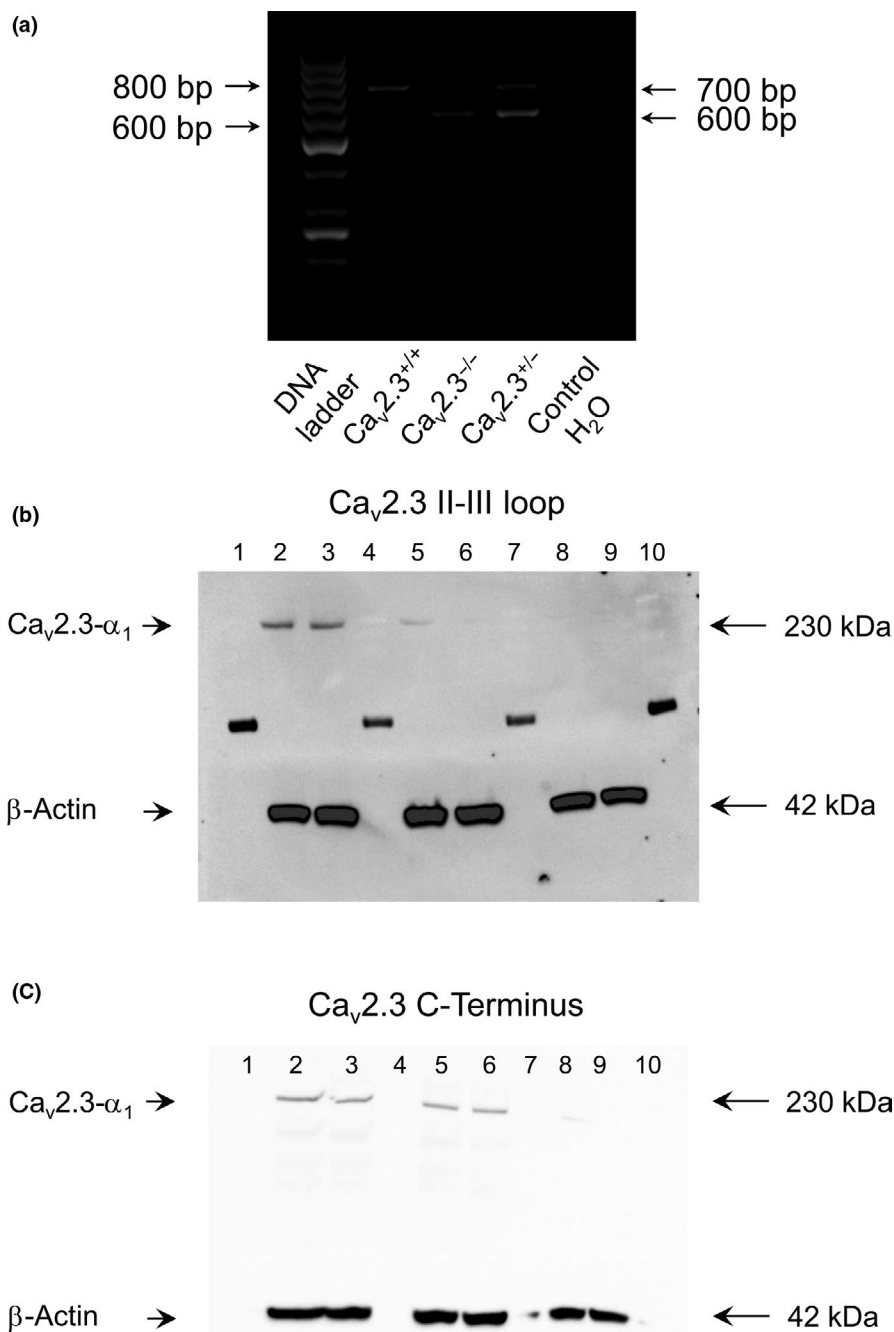

FIGURE 1 Genotyping and Western blot analysis of $Ca_v2.3$ mutant mice. (a) $Ca_v2.3^{+/+}$, $Ca_v2.3^{+/-}$ and $Ca_v2.3^{-/-}$ mice were generated from cryopreserved heterozygous embryos (Wilson et al., 2000). Offspring chromosomal DNA was extracted from tail biopsies for subsequent genotyping. Amplification in $Ca_v2.3^{+/+}$ resulted in a ~700-bp fragment and a ~600-bp fragment in $Ca_v2.3$-deficient ($Ca_v2.3^{-/-}$) mice. In heterozygous $Ca_v2.3^{+/-}$ mice, both fragments were detected. (b) Microsomes (50 µg each) from $Ca_v2.3^{+/+}$ (lanes 2 and 3), $Ca_v2.3^{+/-}$ (lanes 5 and 6) and $Ca_v2.3^{-/-}$ (lanes 8 and 9) mice were analysed using a $Ca_v2.3$-specific antibody directed against the II-III-loop of the underlying pore-forming α_1-subunit. $Ca_v2.3^{+/+}$ controls and heterozygous $Ca_v2.3^{+/-}$ mice display a band of the predicted size (230 kDa). β-Actin (42 kDa) was used as a positive control. Lanes 1, 4, 7 and 10 indicate the protein ladder. (c) Microsomes (75 µg each) from $Ca_v2.3^{+/+}$ (lanes 2 and 3), $Ca_v2.3^{+/-}$ (lanes 5 and 6) and $Ca_v2.3^{-/-}$ (lanes 8 and 9) mice were analysed using a $Ca_v2.3$-specific antibody directed against the C-terminus of the underlying pore-forming α_1-subunit. $Ca_v2.3^{+/+}$ controls and heterozygous $Ca_v2.3^{+/-}$ mice display a band of the predicted size (230 kDa). β-Actin (42 kDa) was used as a positive control. Lanes 1, 4, 7 and 10 indicate the protein ladder

snap-frozen in liquid nitrogen. Subsequently, 1 ml of lysis buffer containing 5 mM Tris-HCl, 2 mM EDTA and proteinase inhibitors (cOmplete Protease Inhibitor Cocktail Tablet) (pH 7.4; all components obtained from Sigma-Aldrich) was added to the frozen tissue followed by homogenization using a rotor–stator homogenizer (TissueRuptor, Qiagen) for 20 s. Cortical samples were then centrifuged for 15 min at $500 \times g$ at 4°C (Centrifuge 5417R; Eppendorf), and the supernatant was kept on ice. Homogenization and centrifugation of the remaining pellet were repeated with another 0.5 ml of lysis buffer, and both supernatants from each animal were finally merged. Subsequently, the merged supernatants were centrifuged at $100,000 \times g$ for 40 min at 4°C (Ultracentrifuge Optima L-80XP, Beckman Coulter) and the resulting pellet was solubilized in 250 µl resuspension buffer (containing 75 mM Tris, 12.5 mM $MgCl_2$, 5 mM EDTA and protease inhibitors (cOmplete Protease Inhibitor Cocktail Tablet) (all components obtained from Sigma-Aldrich). Protein concentration was determined using NanoDrop (NanoDrop 1,000 Spectrophotometer; Thermo Fisher), and appropriate microsomal aliquots were stored at −20°C.

For SDS-PAGE and Western blotting, 50 and 75 µg probes of cortical microsomes from each genotype were mixed with pre-heated $2 \times$ Lämmli buffer (Bio-Rad) and loaded to a precast gel (7.5% Mini-PROTEAN TGX Precast Protein Gel, Bio-Rad). SDS-PAGE was carried out in a Mini-PROTEAN Tetra Cell (Bio-Rad) filled with TGS buffer (25 mM Tris, 192 mM glycine, 0,1% SDS, pH 8.3, Bio-Rad). Prior to blotting, the PVDF membrane was activated for 5 min in pure methanol (Sigma-Aldrich). The blotting sandwich made up of sponges, filter papers, membrane and SDS gel was assembled and inserted into a Mini Trans-Blot Cell (Bio-Rad). The individual components were pre-wetted, and the buffer tank was filled with TG buffer w/o methanol (25 mM Tris, 192 mM glycine, pH 8.3, Bio-Rad). A cooling unit was used to prevent the system from over-heating. Microsomal proteins were blotted for 1 hr at 100 V followed by overnight blotting at 30 V at 4°C to allow the transfer of high molecular weight proteins. Following transfer, the PVDF membrane air-dried for 4 hr to enhance protein fixation and was subsequently blocked for 2 hr in TBS-T (Bio-Rad), containing 5% milk powder and 5% goat serum. The membrane was stained with Ponceau S to check for proper protein transfer. In addition, the SDS gel was analysed for remaining proteins by Coomassie Blue staining. After rinsing with TBS-T, the PVDF membrane was separated into two parts (below and above 70kDa) and incubated with the 1st antibody overnight, at 4°C. The upper PVDF membrane, containing proteins larger than 70 kDa, was either incubated with a polyclonal $Ca_v2.3$ C-Term antibody (host: rabbit, mouse reactivity, diluted 1:1,000 in TBS-T; No. ABIN350140, antibodies-on-line.com, Germany) or with a polyclonal $Ca_v2.3$ II-III loop antibody (host: rabbit, mouse reactivity, corresponding to amino acid residues 892–907 of rat $Ca_v2.3$, diluted 1:200 in TBS-T; No. PA5-77300, Thermo Fisher). The lower PVDF membrane, containing proteins <70 kDa, was incubated with the control monoclonal antibody ß-actin (No. ab179467, diluted 1:5,000 in TBS-T, Abcam). Prior and post incubation with the secondary HRP-conjugated antibody (goat-anti rabbit HRP; 1:5,000; Abcam) for 1 hr at RT, the membrane slips were washed 3 times for 10 min in TBS-T using an orbital shaker (SI500, Stuart). Membranes were incubated for 1 min using Super Signal West Pico Plus Chemiluminescent Substrate (Thermo Fisher), and blot exposure was carried out using ChemiDoc Touch (Bio-Rad).

2.4 | ABR recording procedure

Prior to ABR recordings, animals were anesthetized by intraperitoneal (i.p.) injection of ketamine (100 mg/kg body weight, Ketanest® S, 25 mg/ml, Pfizer) and xylazine (10 mg/kg body weight, Rompun® 2%, Bayer Health Care) and placed inside a sound-attenuating cubicle (ENV-018V, Med Association Inc.) lined with an acoustic foam (Figure S1a). Additional technical/experimental details of this ABR approach such as electrical shielding, temperature support for anesthetized animals and protection from corneal desiccation were described in detail previously (Lundt, Seidel, et al., 2019; Lundt, Soos, et al., 2019).

For recording of monaural bioelectrical auditory potentials, subdermal stainless steel electrodes (27GA 12 mm, Rochester Electro-Medical) were inserted at the vertex, axial the pinnae (positive (+) electrode) and ventrolateral of the right pinna (negative (−) electrode) (Figure S1c). The ground electrode was positioned at the hip of the animal (Lundt, Seidel, et al., 2019; Lundt, Soos, et al., 2019). For details on impedance measurement of the electrodes, verification of proper electrode placement/ conductivity, loudspeaker positioning under free field conditions, and programming of stimulus protocols for click and tone bursts including the software used, see Lundt, Seidel, et al. (2019), Lundt, Soos, et al. (2019) (Figure S1b).

ABR data were sampled at 24.4 kHz, and signals were bandpass filtered (high pass 300 Hz, low pass 5 kHz) using a 6-pole Butterworth filter. The individual ABR data acquisition time was 25 ms consisting of a 5-ms baseline period prior to the individual acoustic stimulus onset (pre-ABR baseline) and exceeding the 10-ms ABR section by another 10-ms baseline (post-ABR baseline, Figure S2a) (Lundt, Seidel, et al., 2019; Lundt, Soos, et al., 2019). Click stimuli were used to determine click thresholds, ABR wave I–IV amplitudes and wave I–IV latencies. Tone burst stimuli were utilized to identify frequency-specific hearing thresholds in the individual mouse lines in the frequency range of 1–42 kHz in 6 kHz steps. For averaging, the acoustic stimuli were applied 300 times at a rate of 20 Hz. ABR threshold recordings were carried out in the increasing SPL mode, that is in 5 dB steps

for clicks and 10 dB steps for tone bursts, ranging from 0 to 90 dB. For further details concerning calibration of the ABR setup and online confirmation of spectral characteristics of sound stimuli using fast Fourier transformation (FFT), please refer to Lundt, Seidel, et al. (2019), Lundt, Soos, et al. (2019).

2.5 | ABR analysis

2.5.1 | General aspects and software

In this study, we used an automated threshold detection based on previous publications (Alvarado, Fuentes-Santamaria, Gabaldon-Ull, Blanco, & Juiz, 2014; Bogaerts, Clements, Sullivan, & Oleskevich, 2009; Probst et al., 2013). Software "R" (The R Foundation, version 3.2.1, R Core Team 2015) was combined with the additional packages "reshape2" (version 1.4.1), "ggplot2" (version 1.0.1), "data.table" (version 1.9.4), "gdata" (version 2.13.3), "pastecs" (version 1.3.18), "waveslim" (version 1.7.5) and "MassSpecWavelet" (version 1.30.0; Du, Kibbe, & Lin, 2006) for data processing and analysis. Wavelet analysis was carried out using "MassSpecWavelet" package (Du et al., 2006; Lundt, Seidel, et al., 2019).

2.5.2 | Analysis of hearing thresholds

To characterize the click and tone burst-derived thresholds of ABR recordings, three distinct time windows (TWs) were defined to calculate the signal-to-noise ratio (SNR): TW_1 (0–5 ms), TW_2 (5–15 ms) and TW_3 (15–25 ms). For the calculation of noise standard deviation of the baseline, ABR trace resetting and definition of ABR hearing thresholds, see Lundt, Seidel, et al. (2019), Lundt, Soos, et al. (2019) and Figure S2a.

2.5.3 | ABR wave amplitude and wave latency analysis

For determination of positive (p) waves (peaks, see intercept points of red-grey lines with ABR trace) and negative (n) waves (pits, see intercept points of blue-orange lines with ABR trace, Figure S2b), a wavelet-based approach was carried out utilizing the "Mexican hat" wavelet which uses a default wavelet by the continuous wavelet transform (CWT)-based pattern-matching algorithm (Du et al., 2006) related to the following equation (Daubechies, 1992):

$$C(a,b) = \int_R S(t)\psi_{a,b}(t)dt, \psi_{a,b}(t) = \frac{1}{\sqrt{a}}\psi\left(\frac{t-b}{a}\right),$$
$$a \in R^+ - \{0\}, b \in R,$$

where *s(t)* is the signal, *a* is the scale, *b* is the translation, *ψ(t)* is the mother wavelet, *ψ*$_{a,b}$*(t)* is the scaled and translated wavelet and *C* is the 2D matrix of wavelet coefficients.

A detailed description of this automated tool for ABR analysis is given in Lundt, Seidel, et al. (2019), Lundt, Soos, et al. (2019). It allows for amplitude growth function analysis and latency comparison of all waves (W_{I-IV}), identifying maximum amplitudes (Figure S2b, green crosses) and mean latencies (Figure S2b, red-grey lines) of each of the four p-peaks within the time frame of the related n-peaks. Note that all results based on the self-programmed automatic wavelet tool were visually checked afterwards. In rare cases, individual ABR runs were excluded from statistics due to, for example, noise contamination (Lundt, Seidel, et al., 2019; Lundt, Soos, et al., 2019).

2.6 | Real-time PCR of Ca$_v$2.3 mutant mouse cochlea

qPCR was carried out in male and female Ca$_v$2.3$^{+/+}$, Ca$_v$2.3$^{+/-}$ and Ca$_v$2.3$^{-/-}$ mice to identify potential alterations in cochlear transcript levels of other VGCCs (i.e. HVA L-type Ca$_v$1.2 and Ca$_v$1.3, LVA T-type Ca$_v$3.1, Ca$_v$3.2 and Ca$_v$3.3) that were previously reported to be expressed within the cochlea and the auditory tract. For each genotype, the following subgroup was used for analysis: Ca$_v$2.3$^{+/+}$: ♂, $n = 8$, 21.23 ± 0.16 weeks; ♀, $n = 8$, 21.54 ± 0.32 weeks; Ca$_v$2.3$^{\pm}$: ♂, $n = 8$, 20.71 ± 0.14 weeks; ♀, $n = 8$, 22.25 ± 0.61 weeks; Ca$_v$2.3$^{-/-}$: ♂, $n = 8$, 20.98 ± 0.25 weeks; ♀, $n = 6$, 21.91 ± 0.50 weeks. Notably, experimental animals for cochlear qPCR analysis were not used in ABR experiments before. Both cochleae of each individual animal were dissected in an RNase-free environment (RNAlater stabilization reagent, Qiagen) and snap-frozen in liquid nitrogen. Total RNA from both mouse cochleae was extracted using Direct-zol RNA Micro Kit (Zymo Research, Freiburg i.Br.) followed by an additional step of DNase digest (Turbo DNA-free Kit, Ambion^{TM}, Thermo Fisher Scientific). Quality and quantity of total RNA were evaluated using the NanoDrop standard procedures (NanoDrop1000, Thermo Fisher Scientific). cDNA synthesis was carried out using a two-step RT-PCR approach using both random hexamer and anchored-oligo(dt)$_{18}$ primers with 250 ng of total cochlea RNA from each animal for the final 50 µl first-strand cDNA mix (Transcriptor First-Strand cDNA synthesis Kit, Roche). cDNA (2 µl) served as template for qPCR (see below), and signal detection was based on SYBR Green I Master (Roche). qPCR experiments were performed using a LightCycler 480 System (Roche) with the following protocol (per cycle) being applied for all primer pairs (Table 1): 95°C (10 min, pre-incubation step); 95°C (10 s, denaturation step); 60°C (20 s, annealing step); and 72°C (30 s, extension step). In total, 40 cycles were performed.

TABLE 1 Characteristics of primer pairs used for qPCR. Real-time PCR for various HVA L-type ($Ca_v1.2$, $Ca_v1.3$) and LVA T-type Ca^{2+} channels ($Ca_v3.1$, $Ca_v3.2$, $Ca_v3.3$) was performed using gene-specific primer pairs. Primer pairs were generated by OriGene Technologies[a] or adapted from Weiergräber et al., 2005[b]

Gene	Protein	Forward sequence (5′–3′)	Reverse sequence (5′–3′)
Cacna1c[a]	$Ca_v1.2 \ \alpha_1$	CGTTCTCATCCTGCTCAACACC	GAGCTTCAGGATCATCTCCACTG
Cacna1d[a]	$Ca_v1.3 \ \alpha_1$	CTACCGTTGCACAGATGAAGCC	TCACGGACCACAGGACTGTCAA
Cacna1g[a]	$Ca_v3.1 \ \alpha_1$	GACCATGTGGTCCTCGTCATCA	TTTCAGCCAGGAAGACTGCCGT
Cacna1h[a]	$Ca_v3.2 \ \alpha_1$	GCACAAAGTGCTGGAGCCCTAT	GTGTGCGATGACTTTCTGGCAG
Cacna1i[a]	$Ca_v3.3 \ \alpha_1$	GTCTTCACCAAGATGGACGACC	ACTTCGCACCAGTCAGGCTTGT
Hprt[b]	HPRT	GCTGGTGAAAAGGACCTCT	CACAGGACTAGAACACCTGC

All cochlea samples were tested in triplicates, and two negative controls in duplicates (no template; no RT) were added to the qPCR 96-well-plate (Roche). Furthermore, cochlea cDNA derived from C57BL/6J mice served as positive control and calibrator cDNA (again in triplicates in every plate) to avoid inter-run variations and guarantee statistical comparability among the plates. Amplification specificity was verified by melting curve analysis (LightCycler 480 System Software, Roche). Deionized, nuclease-free water (no cDNA) and total RNA samples (without RT) were used as controls and HPRT served as internal reference gene. The LightCycler 480 System software (Roche) was used to calculate the Ct-values (cycle threshold) (Lundt, Seidel, et al., 2019; Lundt, Soos, et al., 2019).

Considering the individual primer efficiency, analysis and qPCR statistics were carried out using qBase + qPCR analysis software (Biogazelle) which is based on a delta-Cq quantification model with PCR efficiency correction, reference gene normalization and inter-run calibration (Hellemans, Mortier, Paepe, Speleman, & Vandesompele, 2007). The results were depicted as CNRQ (Calibrated Normalized Relative Quantity) and statistically analysed using the Mann–Whitney test (Lundt, Seidel, et al., 2019; Lundt, Soos, et al., 2019).

2.7 | Statistical analysis

All results in this study are presented as group means ± *SEM* using GraphPad Prism 6 software (V6.07 GraphPad Software, Inc.). Both genders were analysed separately. Statistical differences were compared with an ordinary one-way ANOVA for click-evoked hearing thresholds analysis (Figure 4) and differences in W_{I-IV} interwave intervals (IWI, Figure 7) by Tukey's multiple comparisons test. Two-way repeated-measure ANOVA followed by Tukey's adjustment for multiple comparisons was performed to evaluate differences in tone burst-evoked hearing thresholds (Figure 5a,b) and to calculate amplitude growth function differences (Figure 6). To test statistical significances, we used α-level = 0.05 and p-values defined as *$p < .05$; **$p < .01$; ***$p < .001$; ****$p < .0001$. Note that asterisks indicate significant differences between controls and mutant ($Ca_v2.3^{+/-}$ or

$Ca_v2.3^{-/-}$) mice, whereas "+" icons represent significant differences between heterozygous and knockout animals.

3 | RESULTS

3.1 | Developmental aspects in $Ca_v2.3$ mutant mice

Western blot analysis was used to confirm deletion of the $Ca_v2.3$ protein in $Ca_v2.3$-deficient mice compared with wild-type animals (Figure 1b,c). Cortex preparations from both $Ca_v2.3^{+/+}$ and $Ca_v2.3^{+/-}$ mice displayed a clear band at 230 kDa, the predicted size for the $Ca_v2.3 \ \alpha_1$ subunit (Figure 1b,c). In cortical probes from $Ca_v2.3^{-/-}$ mice, a corresponding band was not observed, indicating the absence of the $Ca_v2.3 \ \alpha_1$ subunit in these animals (Figure 1b,c). $Ca_v2.3$-deficient mice (Figure 1) were reported to exhibit complex physiological alterations (Chen et al., 2000; Dietrich et al., 2003; Kuzmiski et al., 2005; Matthews et al., 2007; Muller et al., 2012; Siwek et al., 2014; Tai et al., 2006; Weiergraber, Henry, et al., 2006a; Weiergraber et al., 2007, 2005, 2010; Weiergraber, Kamp, et al., 2006b; Yang & Berggren, 2005; Yokoyama et al., 2004). Given these phenotypic characteristics of $Ca_v2.3$ null mutants, we first investigated potential developmental alterations in body weight in female and male controls (♀, $n = 9$; ♂, $n = 9$), $Ca_v2.3^{+/-}$ mice (♀, $n = 10$; ♂, $n = 9$) and $Ca_v2.3^{-/-}$ (♀, $n = 11$; ♂, $n = 10$) animals aged 140 – 142 days. In females, no significant change in body weight was observed for $Ca_v2.3^{+/-}$ or $Ca_v2.3^{-/-}$ mice compared with controls at the age of 20 weeks ($Ca_v2.3^{+/+}$, 25.4 ± 0.5 g; $Ca_v2.3^{+/-}$, 25.4 ± 1.3 g; $Ca_v2.3^{-/-}$, 27.0 ± 0.4 g; Figure S3a). The same held true for male controls ($Ca_v2.3^{+/+}$, 32.7 ± 1.7 g), heterozygous ($Ca_v2.3^{+/-}$, 31.6 ± 1.1 g) and homozygous $Ca_v2.3$ null mutants ($Ca_v2.3^{-/-}$, 31.1 ± 0.8 g, Figure S3a). Long-term monitoring revealed reduced body weight in female $Ca_v2.3^{+/-}$ mice compared with controls between 25 and 35 weeks of age (Figure S3b) which did not hold true for male $Ca_v2.3$ heterozygous mutants between 25 and 35 weeks of age (Figure S3c). Note, that ANOVA testing for the total range (5–50 weeks of age) revealed no significant differences.

3.2 | Click- and tone-evoked ABRs in control, $Ca_v2.3^{+/-}$ and $Ca_v2.3^{-/-}$ mice

To get a closer insight into the functional involvement of $Ca_v2.3$ VGCCs in auditory information processing, we performed click- and tone burst-evoked ABR recordings and analysis of hearing thresholds, amplitude growth functions and latencies in controls, $Ca_v2.3^{+/-}$ and $Ca_v2.3^{-/-}$ mice.

Special attention was payed to gender-specific differences, as gender is of major influence in auditory profiling in both men (Murphy & Gates, 1997; Pearson et al., 1995) and mice (Henry, 2004; Ison, Allen, & O'Neill, 2007). ABRs to free
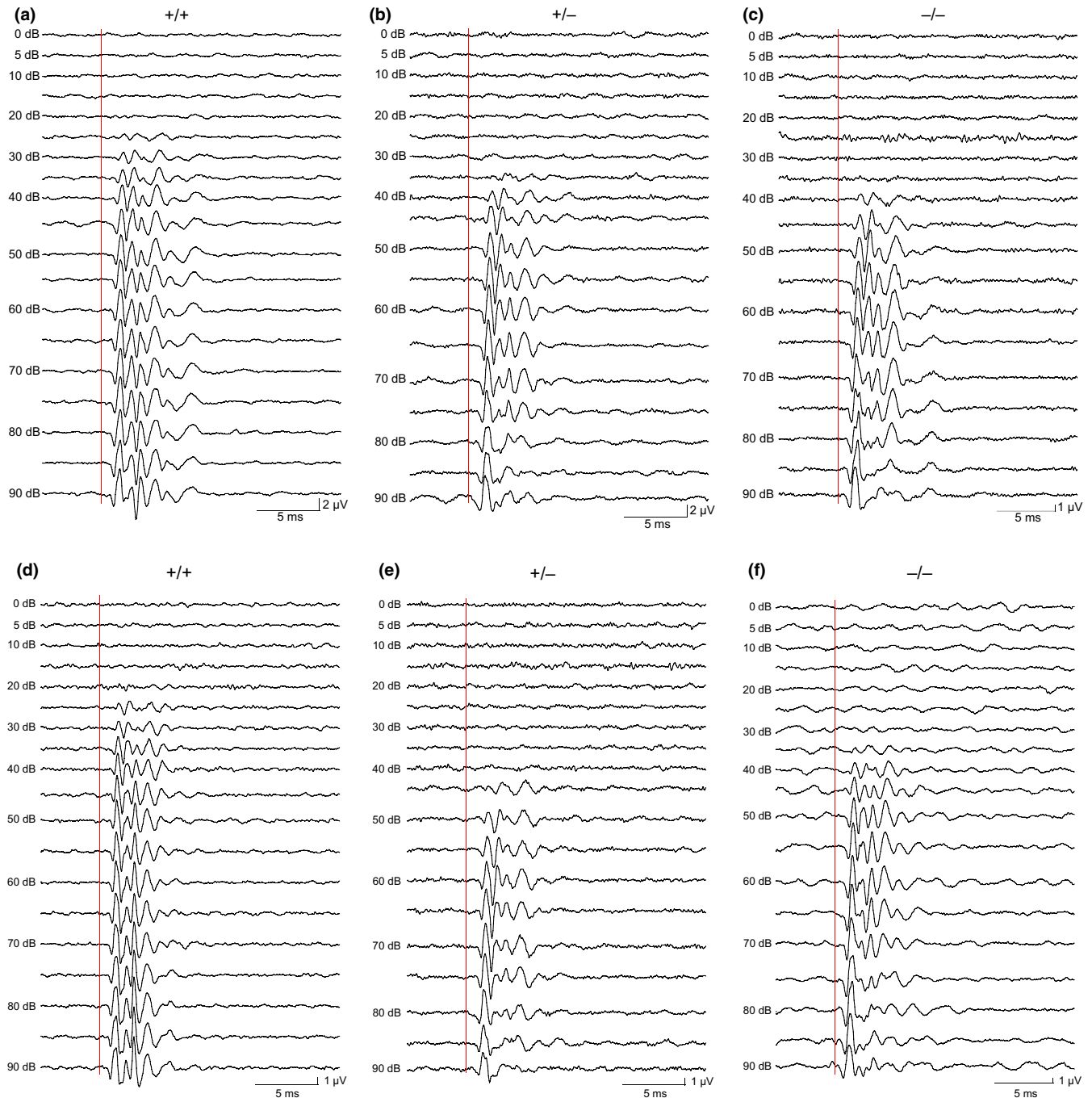

FIGURE 2 Representative ABRs to click stimuli in female and male $Ca_v2.3$ mutant mice. ABRs obtained from female $Ca_v2.3^{+/+}$(a), $Ca_v2.3^{+/-}$ (b) and $Ca_v2.3^{-/-}$ (c) mice as well as male $Ca_v2.3^{+/+}$(d), $Ca_v2.3^{+/-}$ (e) and $Ca_v2.3^{-/-}$ (f) animals upon click stimulation (increasing SPL from 0 to 90 dB with 5 dB SPL steps). Each stimulus entity is presented 300 times at 20 Hz for averaging. The red line indicates the onset of the acoustic stimulus. Note that ABR hearing threshold is increased in female $Ca_v2.3^{+/-}$ mice (see also Figure 4a) and that wave amplitudes are reduced in mutant mice, particularly in $Ca_v2.3^{-/-}$ (see adapted scaling in C, also Figure 6). In males, the ABR hearing threshold is increased in $Ca_v2.3^{+/-}$ mice compared with controls (see also Figure 4b) [Colour figure can be viewed at wileyonlinelibrary.com]

field click (0.1 ms) and pure tone burst (1–42 kHz in 6 kHz steps, 4.5 ms in total with a 1.5-ms ramp time) acoustic stimuli were recorded with subdermal steel electrodes (for electrode positioning, see Materials and Methods). Note that vertex positive deflections are plotted as upward deflections as depicted in representative click-evoked recordings for female $Ca_v2.3^{+/+}$ (Figure 2a), $Ca_v2.3^{+/-}$ (Figure 2b) and $Ca_v2.3^{-/-}$ mice (Figure 2c). Representative ABR recordings in females suggest increased click-evoked ABR thresholds in $Ca_v2.3^{+/-}$ mice and alterations in amplitude growth function (for details, see below). Similarly, representative ABR recordings in males suggested increased click-evoked ABR threshold and altered amplitudes in $Ca_v2.3^{+/-}$ mice (Figure 2e) compared with $Ca_v2.3^{+/+}$ controls (Figure 2d) and $Ca_v2.3$ null mutants (Figure 2f, for details, see below). Representative tone burst-evoked ABRs for females are depicted in Figure 3a–c and for males in Figure 3d–f. Notably, the representative ABR recordings

suggest frequency-specific hearing threshold alterations in both $Ca_v2.3^{+/-}$ (Figure 3b,e) and $Ca_v2.3^{-/-}$ mice (Figure 3c,f).

3.3 | Click-related hearing thresholds in control, $Ca_v2.3^{+/-}$ and $Ca_v2.3^{-/-}$ mice

To evaluate the effect of the $Ca_v2.3$ allelic loss on general hearing performance, we recorded click-evoked ABRs for different SPLs (0–90 dB) in all three genotypes at an age of 140–142 days (~20 weeks). Ordinary one-way ANOVA and a Tukey multiple comparisons test revealed a significant increase ($F_{2,27} = 3.508$, $p = .04$) in click-evoked hearing thresholds for $Ca_v2.3^{+/-}$ female mice (38.50 ± 1.50 dB SPL, $n = 10$) compared with control females (31.67 ± 2.36 dB SPL, $n = 9$, Figure 4a). Similarly, male $Ca_v2.3^{+/-}$ mice (38.89 ± 1.62 dB SPL, $n = 9$) revealed a significant difference ($F_{2,25} = 4.317$, $p = .02$) compared with control males (30.56 ± 2.27 dB SPL,
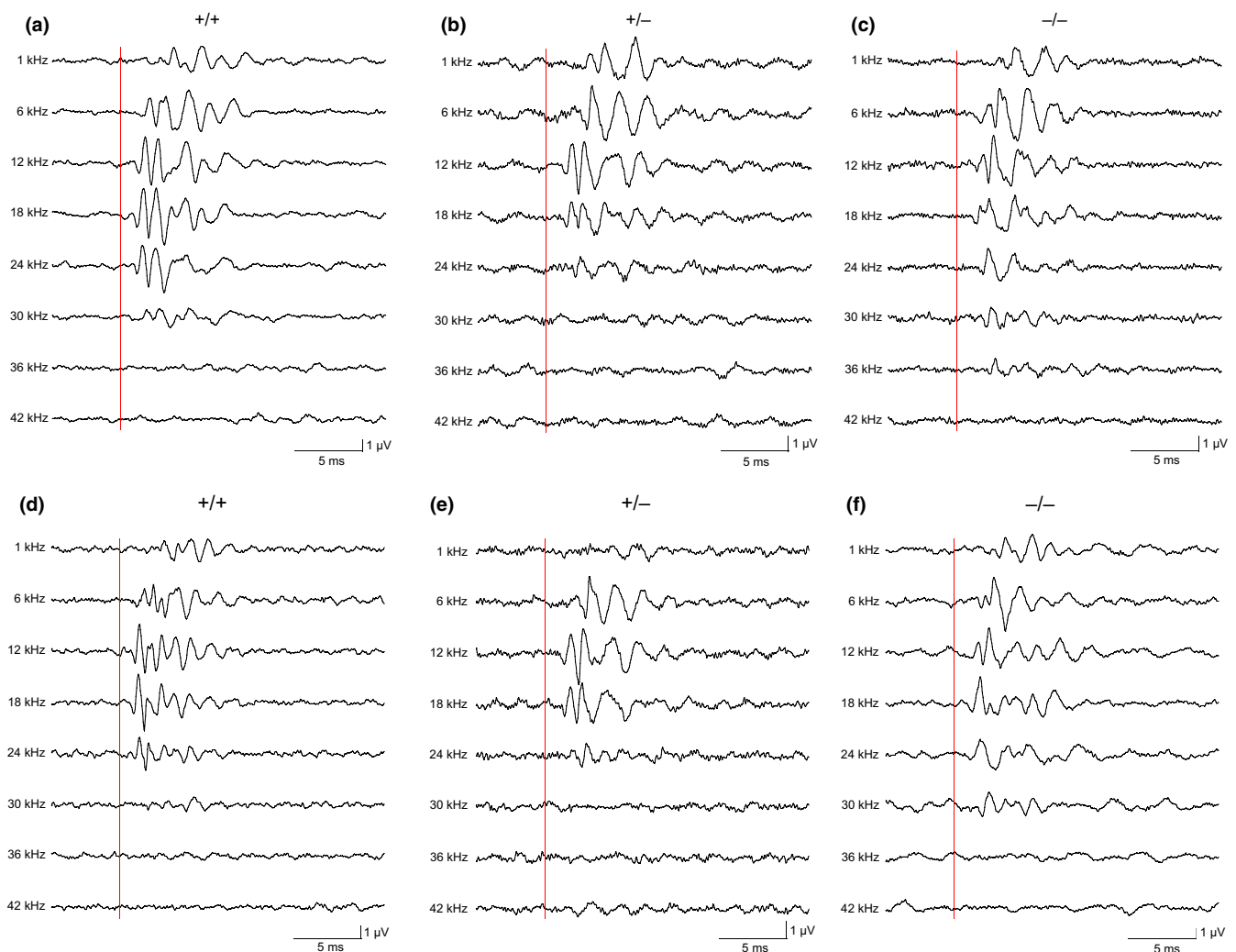

FIGURE 3 ABRs to tone burst stimuli in female and male $Ca_v2.3$ mutant mice. Representative ABRs from female $Ca_v2.3^{+/+}$ (a), $Ca_v2.3^{+/-}$ (b) and $Ca_v2.3^{-/-}$ (c) mice as well as male $Ca_v2.3^{+/+}$ (d), $Ca_v2.3^{+/-}$ (e) and $Ca_v2.3^{-/-}$ (f) animals following tone bursts of 1–42 kHz (6 kHz steps) with an SPL of 80 dB. Each stimulus entity is presented 300 times at 20 Hz for averaging. The red line indicates the onset of the acoustic stimulus. Note that ABR wave amplitudes are reduced in female $Ca_v2.3^{+/-}$ mice at higher frequencies > 30 kHz [Colour figure can be viewed at wileyonlinelibrary.com]

$n = 9$, Figure 4b). No significant differences were found for $Ca_v2.3^{-/-}$ mice ($\female$, 36.82 ± 1.69 dB SPL, $n = 11$; $\male$, 36.50 ± 2.11 dB SPL, $n = 10$). Note that no gender-specific alterations in hearing thresholds were observed between the individual genotypes ($Ca_v2.3^{+/+}$, $Ca_v2.3^{+/-}$ and $Ca_v2.3^{-/-}$) at the age of 20 weeks.

3.4 | Tone burst-related hearing thresholds in control, $Ca_v2.3^{+/-}$ and $Ca_v2.3^{-/-}$ mice

To determine potential alterations in ABR threshold levels evoked by different tone burst frequencies (1–42 kHz, Figure 5a,b), we performed repeated two-way ANOVA followed by a Tukey multiple comparisons test. Significant interaction was obtained regarding genotypes and stimulus frequencies ($\female$: $F_{14,189} = 3.478$, $p = .0001$; $\male$: $F_{14,161} = 2.725$, $p = .001$), whereas there was no significant effect of the genotype on threshold levels. Multiple comparison revealed several significant alterations for individual stimulus frequencies with heterozygous $Ca_v2.3^{+/-}$ mice exhibiting increased ABR thresholds compared with controls, particularly in the range of 6–18 kHz (Figure 5a,b). The percentage of mice with a detectable hearing threshold for the individual frequencies is displayed in Figure 5c,d. The binary response variable "hearing" (yes/no) was analysed with a generalized linear mixed effects model using a logit link (generalized logistic regression), accounting for fixed effects "frequency" (continuous), "group" ($Ca_v2.3^{+/+}$, $Ca_v2.3^{+/-}$, $Ca_v2.3^{-/-}$) and "sex" (male and female) and a random effect "animal." There was no significant gender effect (OR = 1.19; $p = .6$). In addition, no group-specific differences were detected for $Ca_v2.3^{-/-}$ versus $Ca_v2.3^{+/-}$ (OR = 2.18; 95% confidence interval 0.77, 6.13; $p = .140$) and $Ca_v2.3^{+/-}$ versus $Ca_v2.3^{+/+}$ (OR = 2.05; 95% confidence interval 0.77, 5.45; $p = .148$). A significant difference was observed for $Ca_v2.3^{-/-}$ versus $Ca_v2.3^{+/+}$ (OR = 4.47; 95% confidence interval 1.59, 12.54; $p = .0045$).

3.5 | Click-evoked ABR amplitude growth function analysis

In response to moderate to high-intense clicks, there may occur up to six ABR peaks (W_I - W_{VI}) in mice which are assumed to be related to the following neuroanatomical structures: W_I, auditory nerve (distal portion, within the inner ear); W_{II}, cochlear nucleus (proximal portion of the auditory nerve, brainstem termination); W_{III}, superior olivary complex (SOC); W_{IV}, lateral lemniscus (LL); W_V, termination of the lateral lemniscus (LL) within the inferior colliculus (IC) on the contralateral side; W_{VI}, thalamus (medial geniculate body) (Kallstrand, Lewander, Baghdassarian, & Nielzen, 2014; Knipper, Dijk, Nunes, Ruttiger, & Zimmermann, 2013). Notably, the exact association of ABR-related waves II–IV and potential underlying neuroanatomical structures of the ascending auditory pathway is to some extend still a matter of debate.

In 19% of all click-evoked ABR recordings, automated wavelet analysis detected six distinct positive waves. Five distinct positive waves were observed within 45% of all click-evoked ABR recordings and a minimum of four distinct positive waves in 36% of all recordings within the first 10 ms at an SPL of 55 dB. Based on these findings, we focussed our final analysis on $W_{I–IV}$.

Waves I–IV were determined based on their latencies, for example W_I appeared 1.70 ± 0.16 ms and 1.58 ± 0.14 ms after the acoustic stimulus in female and male controls, respectively; W_{II} after 2.51 ± 0.16 ms in females and 2.39 ± 0.17 ms in males; W_{III} after 3.27 ± 0.16 ms in females and 3.16 ± 0.15 ms in males; and W_{IV} after 4.49 ± 0.20 ms in females and 4.29 ± 0.22 ms in males at an SPL of 55 dB in $Ca_v2.3^{+/+}$ mice aged 140–142 days (see also Figure 7).

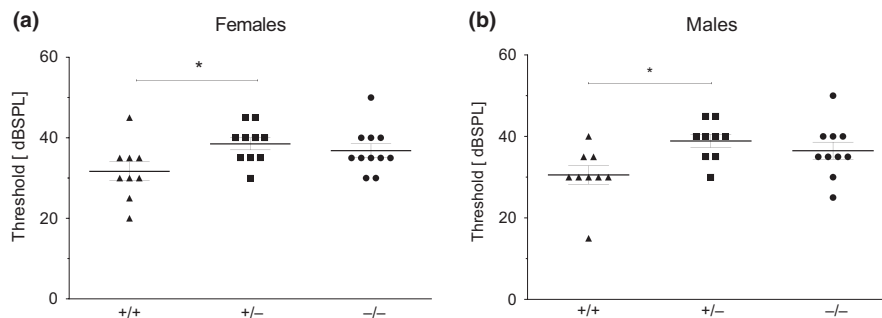ABR amplitude growth function was analysed for W_{I-IV}, and results are depicted in Figure 6. Maximum wave

FIGURE 4 Increased ABR click-evoked hearing thresholds in female and male $Ca_v2.3^{+/-}$ mice. Click-evoked hearing thresholds of female (a) and male (b) $Ca_v2.3^{+/+}$ ($\female$, $n = 9$; $\male$, $n = 9$), $Ca_v2.3^{+/-}$ ($\female$, $n = 10$; $\male$, $n = 9$) and $Ca_v2.3^{-/-}$ ($\female$, $n = 11$; $\male$, $n = 10$) mice aged 140 – 142 days. Hearing thresholds were obtained as described from raw ABR traces (see representative ABR recordings for females and males in Figure 2). One-way ANOVA followed by Tukey multiple comparisons test revealed significant increase in hearing threshold for $Ca_v2.3^{+/-}$ female ($F_{2,27} = 3.508$, $p = .04$) and male ($F_{2,25} = 4.317$; $p = .02$) mice compared with $Ca_v2.3^{+/+}$ female and male animals. Data are presented as scatter plots including mean $\pm$ *SEM*
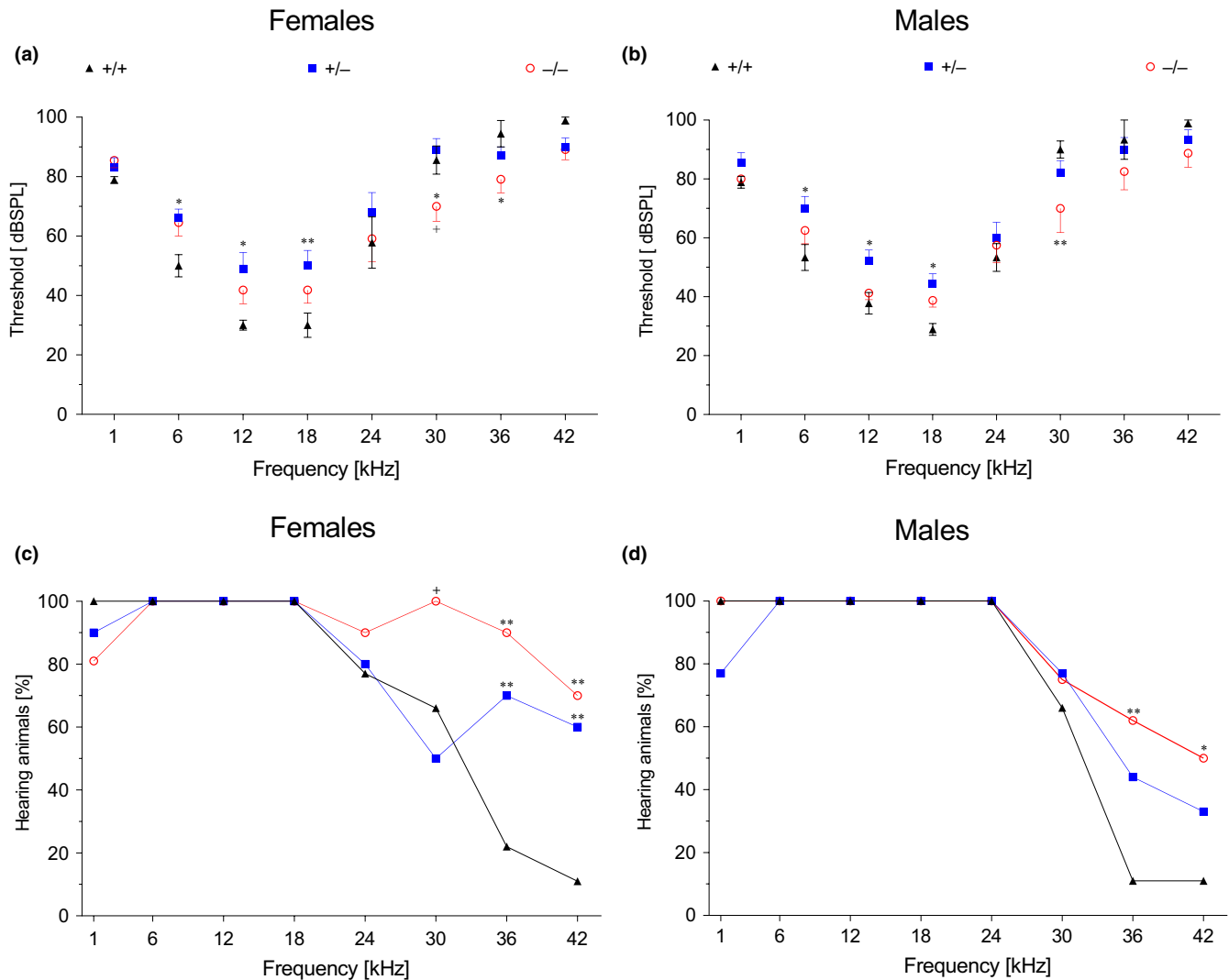
FIGURE 5 Tone burst-evoked ABR hearing thresholds in female and male $Ca_v2.3^{-/-}$ mice. Tone burst (1–42 kHz, 6 kHz steps) evoked ABR-based thresholds for $Ca_v2.3^{+/+}$ (♀, $n = 9$; ♂, $n = 9$, ▲), $Ca_v2.3^{+/-}$ (♀, $n = 10$; ♂, $n = 9$, ■) and $Ca_v2.3^{-/-}$ mice (♀, $n = 11$; ♂, $n = 10$, ○) aged 140 – 142 days (a, b). Hearing thresholds were obtained as described from raw ABR traces (see representative ABR recordings in Figure 3). Significant interaction was found between genotype and stimulus frequency (two-way RM ANOVA; ♀, $F_{14,189} = 3.478$, $p = .0001$; ♂, $F_{14,161} = 2.725$, $p = .001$). Multiple comparison testing revealed several significances for female (a) and male mice (b) for different stimulus frequencies. (c, d) Percentage of mice with a detectable hearing threshold for each frequency. Data were analysed using a generalized logistic regression. No gender effect was detected (OR = 1.19; $p = .6$). A significant group difference was observed for $Ca_v2.3^{-/-}$ versus $Ca_v2.3^{+/+}$ (OR = 4.47; 95% confidence interval 1.59, 12.54; $p = .0045$). Data are depicted as mean ± *SEM*. Asterisks (*) indicate significant differences between mutant mice ($Ca_v2.3^{+/-}$, $Ca_v2.3^{-/-}$) and $Ca_v2.3^{+/+}$ control animals, and "+" icon symbolizes significant differences between $Ca_v2.3^{+/-}$ and $Ca_v2.3^{-/-}$ mice [Colour figure can be viewed at wileyonlinelibrary.com]

amplitudes were plotted against SPL levels tested to unravel potential alterations in wave amplitude growth function over stimulus intensity. Due to the nonexistence or rare appearance of deflections (waves) for low SPL (0–25 dB), wavelet analysis detected no or only limited confirmed accordance of waves in this SPL range. For higher SPL (30–90 dB), wavelet analysis identified mostly all waves ($W_{I–IV}$) in all experimental animals.

For W_I, regular two-way RM ANOVA revealed significant effects of the genotype for male mice ($F_{2,25} = 4.236$, $p < .026$) and significant interaction between genotype and SPL (♀,

$F_{24,324} = 2.417$, $p = .0003$; ♂, $F_{24,300} = 3.564$, $p < .0001$). Tukey multiple comparisons test revealed significant lower amplitudes for $Ca_v2.3^{+/-}$ female mice (SPL 45, 50, 80, 90 dB) compared with $Ca_v2.3^{+/+}$ control females and significantly lower amplitude values for SPL 80–90 dB in $Ca_v2.3^{+/-}$ compared with $Ca_v2.3^{-/-}$ female mice (Figure 6a). Male $Ca_v2.3^{+/-}$ W_I amplitudes turned out to be significantly lower compared with $Ca_v2.3^{-/-}$ amplitude levels between SPL 50 and 80 dB and $Ca_v2.3^{-/-}$ male mice displayed a significantly higher amplitude for 60 dB SPL compared with $Ca_v2.3^{+/+}$ controls using Tukey multiple comparisons test (Figure 6b).
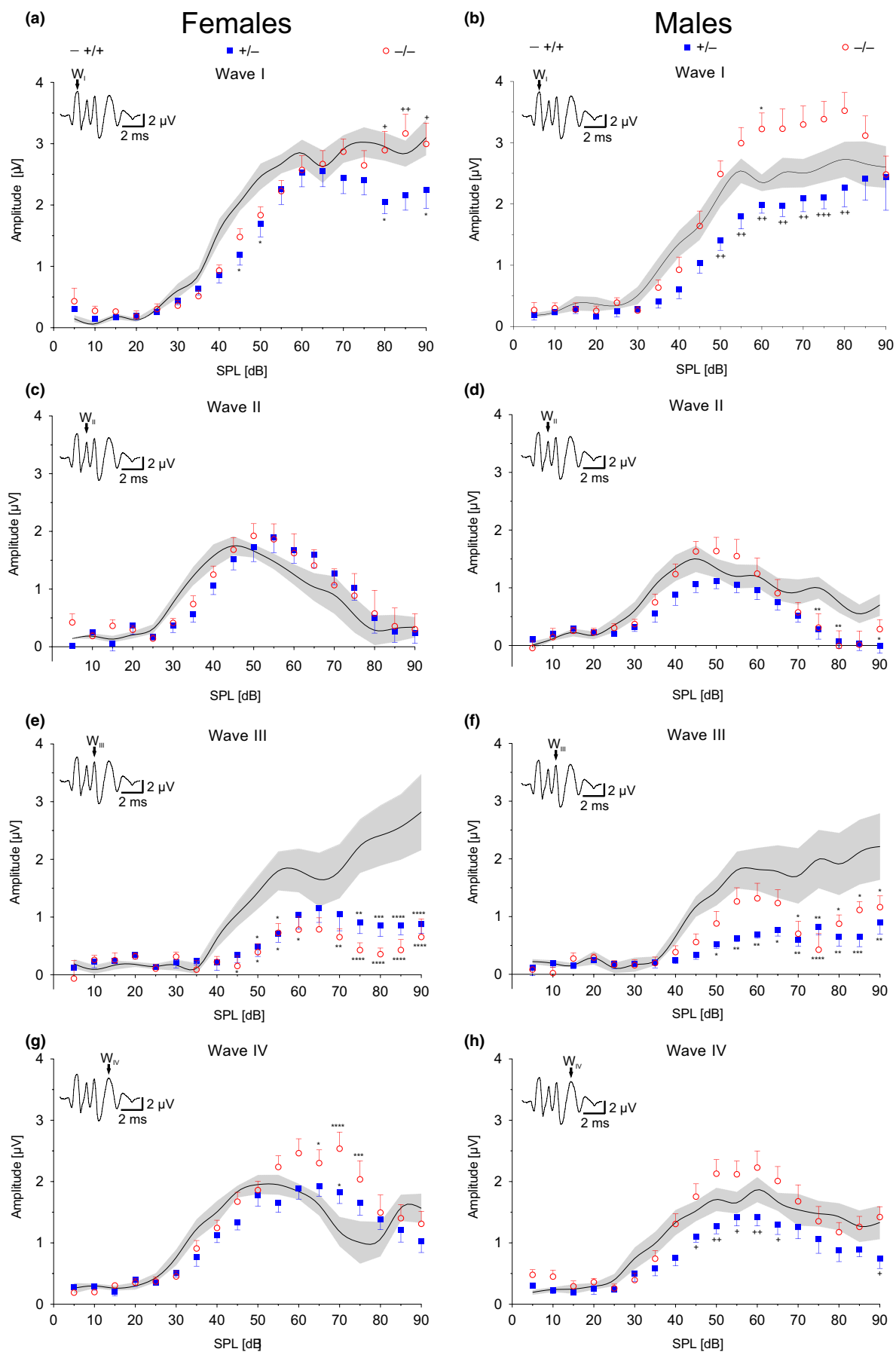
FIGURE 6 Click-evoked ABR amplitude growth function analysis of Waves I–IV for female (left) and male (right) $Ca_v2.3$ mutant mice. Wave I–IV amplitude (µV) plotted against increasing SPL (dB) for click-evoked ABR wave analysis for $Ca_v2.3^{+/+}$ (♀, $n = 9$; ♂, $n = 9$; black line representing the approximated control curve including the 95% confidence interval in grey), $Ca_v2.3^{+/-}$ (♀, $n = 10$; ♂, $n = 9$, ■) and $Ca_v2.3^{-/-}$ mice (♀, $n = 11$; ♂, $n = 10$, ○) aged 140–142 days. $Ca_v2.3^{+/-}$ female and male mice exhibit significant delayed increase in amplitude growth as well as lower maximum amplitudes across the increasing SPL compared with $Ca_v2.3^{+/+}$ mice (a, d, e, f). Significant differences in amplitude growth and maximum amplitude were also found between $Ca_v2.3^{+/-}$ and $Ca_v2.3^{-/-}$ female and male mice (a, b, h). $Ca_v2.3^{-/-}$ animals displayed significantly higher amplitudes compared with $Ca_v2.3^{+/+}$ (b, g) but also significantly lower amplitude (d, e, f). Data are presented as mean ± SEM. Asterisks (*) indicate significant differences between mutant mice ($Ca_v2.3^{+/-}$, $Ca_v2.3^{-/-}$) and $Ca_v2.3^{+/+}$ control animals, and "+" icons indicate significant alterations between $Ca_v2.3^{+/-}$ and $Ca_v2.3^{-/-}$ mice [Colour figure can be viewed at wileyonlinelibrary.com]

No significant differences in W_{II} amplitude growth function were observed in female $Ca_v2.3$ mutant mice (Figure 6c). However, two-way RM ANOVA detected a significant genotype effect ($F_{2,25} = 4.662$, $p = .02$) on the amplitude growth function for W_{II} in male mice (Figure 6d). Tukey multiple comparisons test revealed significant lower amplitude levels for both $Ca_v2.3^{+/-}$ and $Ca_v2.3^{-/-}$ male mice for SPL 75–80 dB and a lower amplitude level of $Ca_v2.3^{+/-}$ male mice for 90 dB SPL (Figure 6d).

Amplitude growth function for W_{III} was significantly affected by genotype (♀, $F_{2,27} = 8.479$, $p = .001$; ♂, $F_{2,25} = 5.931$, $p = .008$) as well as the interaction of the genotype and the stimulation SPL [dB] (♀, $F_{24,324} = 5.255$, $p < .0001$; ♂, $F_{24,300} = 2.578$, $p = .0001$) as determined by two-way RM ANOVA (Figure 6e,f). $Ca_v2.3^{+/-}$ and $Ca_v2.3^{-/-}$ female and male mice display significantly lower amplitude growth and overall amplitude levels compared with $Ca_v2.3^{+/+}$ mice in the range of 45–90 dB SPL as revealed by Tukey multiple comparisons test (Figure 6e,f).

W_{IV} two-way RM ANOVA analysis elicited a significant effect of the genotype on $Ca_v2.3$ male mice ($F_{2,25} = 3.720$, $p = .04$, Figure 6h) and significant interaction of the genotype and stimulus SPL on $Ca_v2.3$ female mice ($F_{24,324} = 4.151$, $p < .0001$, Figure 6g). Significant effects of the SPL on amplitude growth function of $Ca_v2.3$ mutant mice (both ♀ and ♂, $p < .0001$) were observed for all waves (W_{I-IV}) by two-way RM ANOVA (Figure 6a–h). Tukey multiple comparisons test for W_{IV} amplitude shows significantly higher amplitudes between 65 and 75 dB SPL for $Ca_v2.3^{-/-}$ and $Ca_v2.3^{+/-}$ female mice compared with $Ca_v2.3^{+/+}$ female mice (Figure 6g). Significantly different amplitude values were detected between $Ca_v2.3^{+/-}$ and $Ca_v2.3^{-/-}$ male mice between 45 and 65 dB SPL as well as 90 dB SPL using Tukey multiple comparisons test (Figure 6h).

3.6 | Click-evoked ABR waveform latency analysis

In order to investigate the role of $Ca_v2.3$ Ca^{2+} channels on the temporal aspects of auditory information processing within the inner ear and brainstem, we analysed click-evoked wave latencies by measuring the processing time of each ABR wave (W_I-W_{IV}). We also analysed the W_{I-IV} interwave interval (IWI) which reflects the conduction time from cranial nerve VIII (as due to W_I) to the lateral lemniscus (W_{IV}) (Burkard, Eggermont, & Manuel, 2007). Latency analysis was carried out at 55 dB SPL as resultant ABRs provided best fit using the automated complex "Mexican hat"-based wavelet approach.

Importantly, no alterations in absolute W_{I-IV} latencies could be detected for both male and female $Ca_v2.3^{+/-}$ and $Ca_v2.3^{-/-}$ mice. $Ca_v2.3^{-/-}$ female mice, however, displayed a significant increase in W_{I-IV} IWI ($F_{2,27} = 3.938$, $p = .03$) as revealed by unpaired one-way ANOVA with a Tukey multiple comparisons test (♀: $Ca_v2.3^{+/+}$, 2.792 ± 0.045 ms, $n = 9$; $Ca_v2.3^{+/-}$, 2.846 ± 0.031 ms, $n = 10$; $Ca_v2.3^{-/-}$, 2.973 ± 0.059 ms, $n = 11$, Figure 7i). No significant changes were obtained for $Ca_v2.3^{-/-}$ male and $Ca_v2.3^{+/-}$ female or male mice (♂: $Ca_v2.3^{+/+}$, 2.706 ± 0.042 ms, $n = 9$; $Ca_v2.3^{+/-}$, 2.820 ± 0.041 ms, $n = 9$; $Ca_v2.3^{-/-}$, 2.743 ± 0.030, $n = 10$; Figure 7i,j).

In addition, latency analysis was carried out for specific sensation levels, that is 10 and 20 dB above the individual hearing threshold of the experimental animals (data not shown). No statistical alterations were observed under these settings.

3.7 | Cochlear VGCC transcript levels in $Ca_v2.3$ mutant mice

Various VGCCs are expressed in the murine cochlea and ascending auditory pathway including the HVA $Ca_v1.2$ and $Ca_v1.3$ L-type channels, and the LVA T-type channels $Ca_v3.1$–3.3. qPCR was carried out to reveal potential compensatory changes in these channel entities upon mono-allelic or complete $Ca_v2.3$ gene inactivation. Analysis in males revealed no transcriptional changes in these VGCCs in the cochlea of $Ca_v2.3^{+/-}$ and $Ca_v2.3^{-/-}$ mice that could be directly attributed to the observed alterations in click- and tone burst-related hearing thresholds, W_{I-IV} amplitude growth function and W_{I-IV} latencies (Figure 8, see also fold changes and statistics in Table S1). In females however, a significant alteration in $Ca_v3.1$ transcripts between $Ca_v2.3^{+/-}$ and $Ca_v2.3^{-/-}$ mice was detected (HT/KO fold change: -1.572, $p = .03$, Figure 9c, Table S1). In addition, gender differences were observed in $Ca_v2.3^{-/-}$ mice for
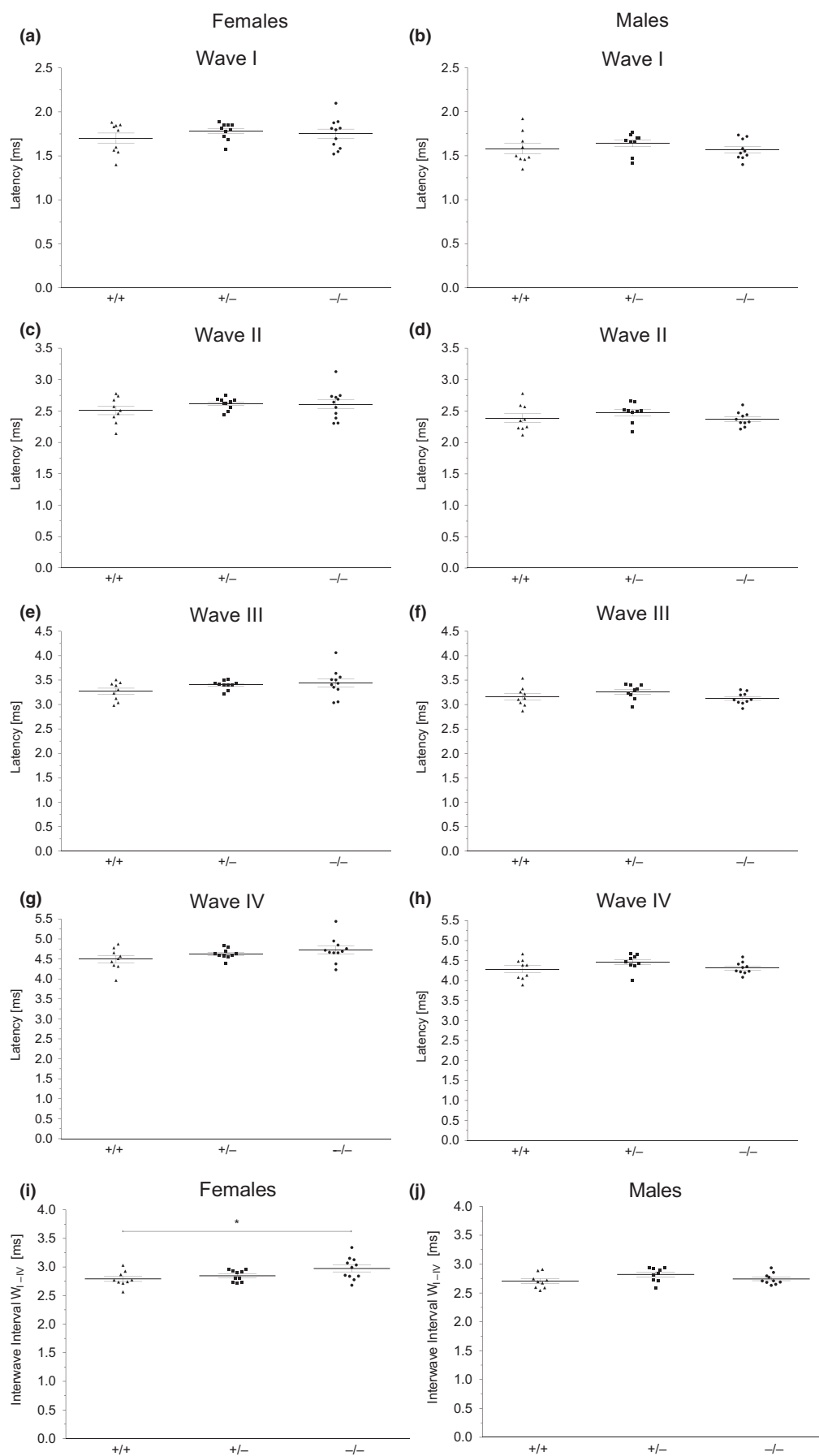
FIGURE 7 Click-evoked ABR latency and interwave interval W_{I-IV} analysis for female and male $Ca_v2.3^{+/+}$, $Ca_v2.3^{+/-}$ and $Ca_v2.3^{-/-}$ mice. Latencies (ms) for each ABR wave (I–IV) at 55 dB SPL are depicted for all three genotypes for both genders ($Ca_v2.3^{+/+}$ (♀, $n = 9$; ♂, $n = 9$; ▲), $Ca_v2.3^{+/-}$ (grey bars, ♀, $n = 10$; ♂, $n = 9$; ■), $Ca_v2.3^{-/-}$ mice (♀, $n = 11$; ♂, $n = 10$; ○); females, a, c, e, g, i; males, b, d, f, h, j). Statistical analysis revealed no differences in absolute $W_I - W_{IV}$ latencies in mutant mice in both females and males (a–h). (i,j) Interwave interval (IWI) W_{I-IV} was analysed at an SPL of 55 dB with mice aged 140–142 days. (i) A significant increase in IWI W_{I-IV} was observed for $Ca_v2.3^{-/-}$ female mice compared with $Ca_v2.3^{+/+}$ female mice using unpaired one-way ANOVA ($F_{2,27} = 3.938$, $p = .03$) followed by a Tukey multiple comparisons test ($p = .03$). (j) No differences in IWI W_{I-IV} were detected in $Ca_v2.3$ male mutant mice. Data are depicted as scatter plots including mean $\pm$ *SEM*

$Ca_v3.1$ (FC ♀/♂ 1.779, $p = .02$) and $Ca_v3.2$ (FC ♀/♂ 2.370, $n = 0.043$) (Table S2).

4 | DISCUSSION

4.1 | Functional implications of $Ca_v2.3$ VGCCs in the inner ear and ascending auditory tract

Our results provide novel insight into the role of $Ca_v2.3$ VGCCs in auditory information processing. Interestingly, increased click-evoked hearing thresholds were detected in heterozygous $Ca_v2.3^{+/-}$ mice but not in $Ca_v2.3^{-/-}$ animals. Similarly, tone burst-evoked hearing thresholds were increased in $Ca_v2.3^{+/-}$ mice in the lower frequency range (8–16 kHz) with no prominent changes in $Ca_v2.3$-deficient animals. Notably, the percentage of hearing animals was increased in both $Ca_v2.3^{+/-}$ and $Ca_v2.3^{-/-}$ mice for tone burst testing in the higher frequency range 36–42 kHz. In addition, complex changes in amplitude growth function were observed in $Ca_v2.3$ mutant animals. Increased hearing thresholds and reduced W_I amplitude in $Ca_v2.3^{+/-}$ mice might point to a functional expression of $Ca_v2.3$ VGCCs in the inner ear, whereas amplitude alterations in W_{III} might originate from the superior olivary complex. As latency analysis of identical sensation levels (10 and 20 dB above the individual hearing thresholds) did not reveal mouse line-specific differences, alterations, particularly in
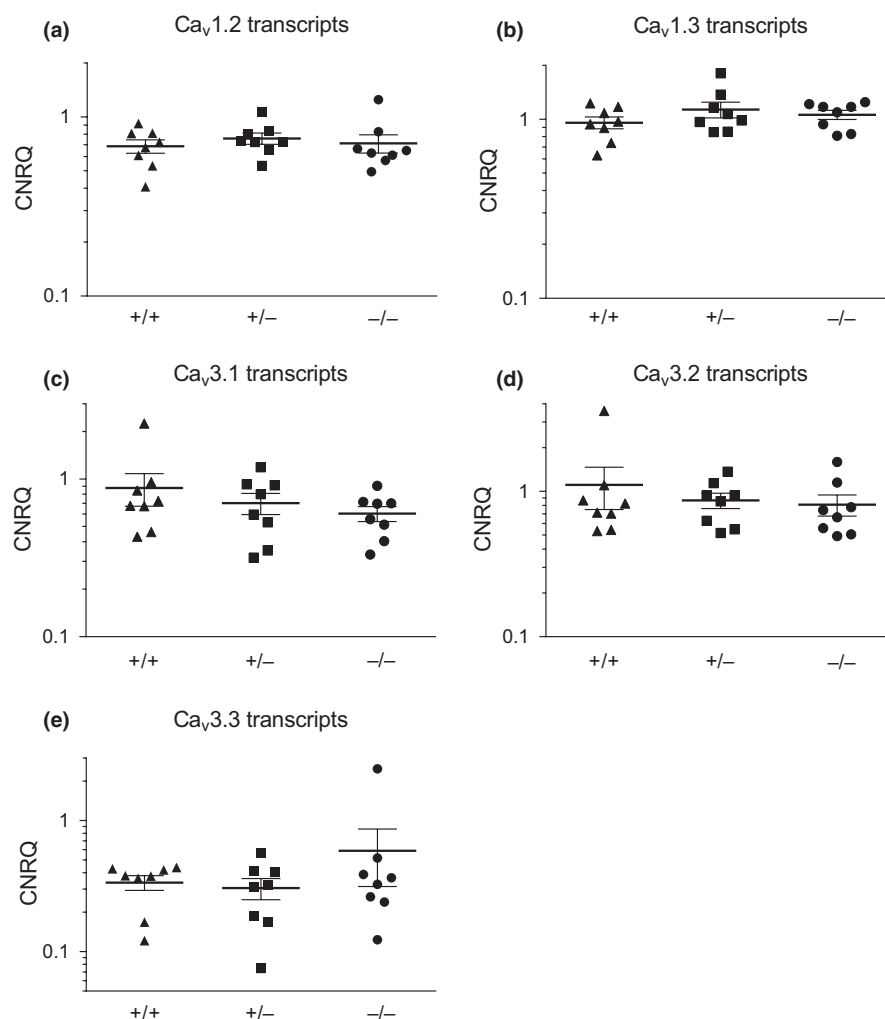

FIGURE 8 Cochlear VGCC transcripts in male $Ca_v2.3$ mutant mice. RNA was isolated from the cochlea of male $Ca_v2.3^{+/+}$ ($n = 8$), $Ca_v2.3^{+/-}$ ($n = 8$) and $Ca_v2.3^{-/-}$ mice ($n = 8$) and utilized in a qPCR approach to check for alterations in other VGCC ($Ca_v1.2$, $Ca_v1.3$, $Ca_v3.1$, $Ca_v3.2$, $Ca_v3.3$) transcript levels. Transcript levels were normalized to the calibrator. No significant changes were observed for the VGCCs tested. CNRQ, calibrated normalized relative quantity. Results are depicted as scatter plots including mean $\pm$ *SEM*
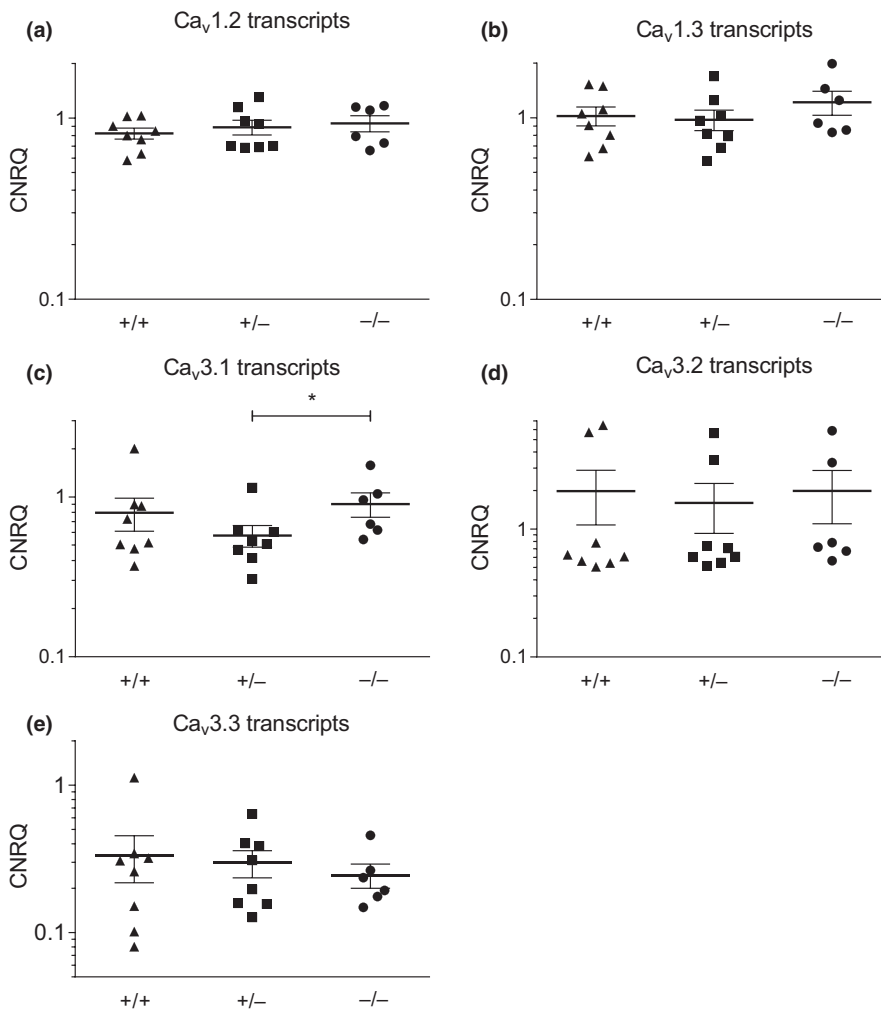
(a) Ca$_v$1.2 transcripts

(b) Ca$_v$1.3 transcripts

(c) Ca$_v$3.1 transcripts

(d) Ca$_v$3.2 transcripts

(e) Ca$_v$3.3 transcripts

FIGURE 9 Cochlear VGCC transcripts in female Ca$_v$2.3 mutant mice. RNA was isolated from the cochlea of female Ca$_v$2.3$^{+/+}$ ($n = 8$), Ca$_v$2.3$^{+/-}$ ($n = 8$) and Ca$_v$2.3$^{-/-}$ mice ($n = 6$) and utilized in a qPCR approach to check for alterations in other VGCC (Ca$_v$1.2, Ca$_v$1.3, Ca$_v$3.1, Ca$_v$3.2, Ca$_v$3.3) transcript levels. Transcript levels were normalized to the calibrator. A significant change was observed for Ca$_v$3.1 VGCCs between heterozygous and Ca$_v$2.3-deficient mice. CNRQ, calibrated normalized relative quantity. Results are depicted as scatter plots including mean $\pm$ *SEM*

Ca$_v$2.3$^{+/-}$ mice, might be related to functional implications of R-type Ca^{2+} channels in the inner ear.

4.2 | Paradoxic genotype–phenotype correlation in Ca$_v$2.3$^{+/-}$ and Ca$_v$2.3$^{-/-}$ mice

In our study, we did not observe a typical gene dose-dependent auditory phenotype in Ca$_v$2.3$^{+/-}$ and Ca$_v$2.3$^{-/-}$ mice. There is often a strong bias in statistics on genotype–phenotype correlation in genetically modified mice due to variable depth of scientific investigation, potential publication restrictions of negative results, etc. (Barbaric, Miller, & Dear, 2007). In about 10%–15% of knockouts generated so far, no overt phenotype could be detected and mutant mice do not seem to exhibit pathophysiological alterations, although one might have expected a severe phenotype based on the reported function of the gene and its expression pattern (Barbaric et al., 2007). In terms of auditory profile, Ca$_v$2.3$^{-/-}$ mice seem to exhibit strong phenotypic and genetic robustness which could be due to compensatory alterations in transcriptional profiles affecting ion channel physiology, signal transduction cascades, and neuronal

degeneration and apoptosis, and which might counteract the deletion of the cacna1e target gene. The mechanisms of such robustness could be dichotomous, that is, by activation of alternative pathways for auditory processing (genetic buffering), or by functional complementation, in which genes are redundant in function to a variable extent (Gu et al., 2003). A lack of a prominent knockout phenotype, as observed in the Ca$_v$2.3$^{-/-}$ auditory profile, could be related to paralogous genetic redundancy (Barbaric et al., 2007) in a complete or partial fashion (Thomas, 1993). Are there other VGCCs that could at least partially mimic the role of Ca$_v$2.3 Ca^{2+} channels in the auditory tract?

4.3 | LVA Ca^{2+} channels in the auditory tract—functional integration of Ca$_v$1.3, Ca$_v$2.3 and Ca$_v$3 VGCCs

Localization studies of Ca$_v$2.3 VGCCs in the inner ear and auditory tract are still fragmentary and partially inconsistent and do not entirely correlate with electrophysiological studies (Bloodgood & Sabatini, 2007; Yokoyama et al., 1995; Zaman et al., 2011). Ca$_v$2.3 channels were reported to be expressed

in the Organ of Corti (Waka et al., 2003), spiral ganglion neurons (SGNs) (Peng et al., 2004), the cochlear nucleus (Bal & Oertel, 2007; Kim & Trussell, 2007; Parajuli et al., 2012), the pontine nuclei, inferior olive, lateral superior olive and the nucleus of the solitary tract (Parajuli et al., 2012; Soong et al., 1993; Williams et al., 1994). Besides $Ca_v2.3$, numerous electrophysiological studies already suggested an important role of low- to mid voltage-activated Ca^{2+} currents in these structures, including $Ca_v1.3$ L-type and Ca_v3 T-type VGCCs: Analysis of $Ca_v1.3^{-/-}$ mice revealed cardiac arrhythmia and deafness (Platzer et al., 2000), secretory and developmental deficits in IHCs and OHCs and alterations in the functional interference with an armamentarium of other voltage- and ligand-gated ion channels, for example, Ca^{2+}-activated K^+ channels (BK, SK), acetylcholine receptors (AChR), $Ca_v1.2$ L-type, $Ca_v2.1$ P/Q and $Ca_v2.2$ N-type VGCCs (Beutner, Voets, Neher, & Moser, 2001; Frank, Khimich, Neef, & Moser, 2009; Glueckert et al., 2003; Goutman & Glowatzki, 2007; Johnson & Marcotti, 2008; Johnson, Marcotti, & Kros, 2005; Kim, Li, & von Gersdorff, 2013; Marcotti, Johnson, Holley, & Kros, 2003; Michna et al., 2003; Moser & Beutner, 2000; Nemzou, Bulankina, Khimich, Giese, & Moser, 2006; Zorrilla de San, Pyott, Ballestero, & Katz, 2010). Electrophysiologically, $Ca_v1.3$ VGCCs were proven to exhibit low- to mid-voltage-activated kinetics in hair cells (Inagaki & Lee, 2013; Zampini et al., 2010). In addition, classical LVA T-type Ca^{2+} channels, such as $Ca_v3.1$ and $Ca_v3.2$, were reported to play an important role in auditory information processing as well (Inagaki et al., 2008; Lei et al., 2011; Lundt, Seidel, et al., 2019; Nie et al., 2008; Shen et al., 2007).

$Ca_v2.3$ VGCCs have exceptional electrophysiological characteristics (Soong et al., 1993; Weiergraber, Kamp, et al., 2006b; Williams et al., 1994) and have attracted specific attention due to their functional involvement in neurotransmitter release (Gasparini, Kasyanov, Pietrobon, Voronin, & Cherubini, 2001; Wu, Westenbroek, Borst, Catterall, & Sakmann, 1999) and synaptic plasticity (Yasuda, Sabatini, & Svoboda, 2003). Thus, the functional implications of $Ca_v2.3$ VGCC in the auditory system are complex. In cellular electrophysiology, $Ca_v2.3$ Ca^{2+} channels can serve as sophisticated tuning elements, acting as low- to mid voltage-activated ion channels capable of triggering or regulating complex cellular firing patterns. The latter includes transition of tonic firing to oscillatory burst like activity and vice versa or modulation of neuronal afterhyperpolarization (Shcheglovitov et al., 2012; Weiergraber, Kamp, et al., 2006b). Both simple and complex action potential (spike) patterns and afterhyperpolarizations in auditory structures require Ca_v3 T-type and $Ca_v2.3$ R-type Ca^{2+} channels in addition to BK and SK channels (Kim & Trussell, 2007). For example, the firing rate of principal neurons in the LSO is a linear function of differences in interaural sound intensity. It has been hypothesized that this linear response results from the functional integration of excitatory ipsilateral and inhibitory contralateral inputs. In the LSO, $Ca_v3.2$ and $Ca_v2.3$ VGCCs were detected and reported to be highly sensitive to Ni^{2+} (Kang et al., 2006) and both might contribute to the complex firing pattern of LSO cells (Jurkovicova-Tarabova et al., 2012). Importantly, $Ca_v2.3$ seems to partially compensate $Ca_v1.3$ ablation in LSO neurons (Jurkovicova-Tarabova et al., 2012). $Ca_v1.3$ VGCCs, which are known to be of central importance in IHCs, display fundamental electrophysiological properties similar to those of typical Ca_v3 LVA channels, such as rapid activation kinetics (Inagaki & Lee, 2013; Koschak et al., 2001; Xu & Lipscombe, 2001; Zampini et al., 2013, 2010). The latter are relevant for the temporal characteristics of sound coding and the ability to accurately trigger auditory nerve firing to reflect sound frequency in terms of phase locking. In immature IHCs, $Ca_v1.3$ VGCCs activate at relatively negative potentials (∼–70 mV) which is a basic electrophysiological property of LVA channels as well (Koschak et al., 2001; Xu & Lipscombe, 2001; Zampini et al., 2010). Therefore, given a resting membrane potential (RMP) of ∼–60 mV in these cells (Marcotti et al., 2003), $Ca_v1.3$ and $Ca_v2.3$ Ca^{2+} channels may support tonic neurotransmitter release at rest and effectively link increased sound pressure levels with higher rates of transmitter release. Mechanistically, $Ca_v2.3$ might contribute to these processes by involvement in the complex spatiotemporal interdependence of intracellular Ca^{2+} levels and Ca^{2+}-activated K^+ currents in HCs in membranaceus nanodomains (Bloodgood & Sabatini, 2007, 2009; Joiner & Lee, 2015; Zaman et al., 2011). In the SGN, inhibition of Ca^{2+} currents resulted in attenuated spontaneous activity and different subtypes of Ca^{2+} currents activated resting outward conductances. Consequently, blockage of these Ca^{2+} currents caused depolarization of the RMP (Lv et al., 2012; Peng et al., 2004). Similarly, in glycinergic interneurons (Cartwheel cells) of the dorsal cochlear nucleus, early complex spike firing patterns were based on $Ca_v2.3$ R-type Ca^{2+} channels together with BK and SK channels (Kim & Trussell, 2007).

Recent expression studies and electrophysiological analysis carried out by Chen et al. (2011) elicited that VGCCs are relevant for neuronal responsiveness in both the high- and low-frequency ranges. This tonotopic specialization is characterized by neurons with rapid kinetic features coding for high-frequency auditory signals and other neurons with slower kinetic features coding for low-frequency auditory signals. Developmental variations in activation and inactivation kinetics along the tonotopic axis enable VGCCs to shape the firing pattern and modulate the unique functional specialization of auditory neurons (Chen et al., 2011). Several VGCCs are expressed in the inner ear and auditory tract. However, $Ca_v2.3$ exhibits the most heterogenous and extraordinary functional expression compared to all other VGCCs (Chen et al., 2011). Besides expression in SGNs, $Ca_v2.3$ VGCCs were also detected in satellite cells, putative myelinating Schwann cells and compact myelin

(Chen et al., 2011) and the density of $Ca_v2.3$ expression was highly variable in these structures. Thus, functional integration of $Ca_v2.3$ Ca^{2+} channels regarding the tonotopic specialization and action potential propagation is most complex and potentially much more sophisticated than for any other VGCC reported so far. Importantly, $Ca_v3.1$ VGCCs exhibited a similar expression compared to $Ca_v2.3$ channels (Chen et al., 2011). This is of high relevance as our qPCR results suggest reduced $Ca_v3.1$ transcript levels in heterozygous $Ca_v2.3^{+/-}$ mice, whereas $Ca_v3.1$ levels in $Ca_v2.3^{-/-}$ female animals remain normal. This points to a potential compensatory mechanism in knockout mice that is not effective in $Ca_v2.3^{+/-}$ animals.

Finally, our observations of unaltered click-evoked hearing thresholds and increased percentage of hearing animals in $Ca_v2.3$-deficient mice could also indicate an overlapping effect of $Ca_v2.3$ ablation on both functional auditory information processing on the one hand and neurodegenerative processes on the other hand. $Ca_v2.3$ VGCCs are involved in excitotoxicity and neurodegeneration, and $Ca_v2.3$-mediated Ca^{2+} influx can trigger neuronal cell death under specific circumstances (Suzuki et al., 2004; Weiergraber et al., 2007). While ablation of $Ca_v2.3$ might thus be critical for proper HC function and synaptic processing in the auditory tract, its ablation might be preservative or neuro-/otoprotective in terms of age-related degeneration of HCs and further structures of the auditory tract and underlines the Janus-like behaviour of $Ca_v2.3$.

4.4 | Perspectives

Future qualitative and quantitative immunohistochemical studies on cochlear hair cells and SGN could prove a potential otoprotective effect of $Ca_v2.3$ ablation in the auditory tract. Assuming that both neuroprotective effects and age-related hearing loss are negligible at early age, ABR studies in young mutant mice might help to further disentangle the complex functional properties of $Ca_v2.3$ in the auditory tract. Finally, cellular electrophysiology will be necessary to characterize the exact cellular mechanistic role of $Ca_v2.3$ VGCCs in the physiology and pathophysiology of the inner ear and peripheral auditory tract. Given the complex findings presented here, $Ca_v2.3$ VGCCs might serve as an important candidate for pharmaceutical interference in the auditory tract in the future.

CONFLICT OF INTEREST

The authors declare that the research was conducted in the absence of any commercial or financial relationships that could be construed as a potential conflict of interest.

AUTHOR CONTRIBUTIONS

Andreas Lundt, Julien Soós performed the experiments and carried out the analysis; Robin Seidel and Ralf Müller analysed the data; Christina Henseler and Varun Raj Ginde performed the experiments; Imran Muhammed Arshaad, Carola Wormuth, Dan Ehninger, Jürgen Hescheler and Agapios Sachinidis drafted the paper, and contributed to the technical/methodological optimization and validation; Karl Broich and Carola Wormuth drafted the paper; Anna Papazoglou analysed the data and drafted the paper; Marco Weiergräber carried out project management, designed the study, analysed the data and drafted the paper.

DATA AVAILABILITY STATEMENT

Primary click- and tone burst-evoked ABR data from all three mouse lines ($Ca_v2.3^{+/+}$, $Ca_v2.3^{+/-}$ and $Ca_v2.3^{-/-}$) from both genders are archived in the Mendeley repository (DIO: (https://doi.org/10.17632/g6ygz2spzx.1), URL: (https://data.mendeley.com/datasets/g6ygz2spzx/1)).

ORCID

Marco Weiergräber https://orcid.org/0000-0002-6058-4752

REFERENCES

Alvarado, J. C., Fuentes-Santamaria, V., Gabaldon-Ull, M. C., Blanco, J. L., & Juiz, J. M. (2014). Wistar rats: A forgotten model of age-related hearing loss. *Frontiers in Aging Neuroscience*, 6, 29. https://doi.org/10.3389/fnagi.2014.00029

Bal, R., & Oertel, D. (2007). Voltage-activated calcium currents in octopus cells of the mouse cochlear nucleus. *Journal of the Association for Research in Otolaryngology*, 8, 509–521.

Barbaric, I., Miller, G., & Dear, T. N. (2007). Appearances can be deceiving: Phenotypes of knockout mice. *Briefings in Functional Genomics and Proteomics*, 6, 91–103. https://doi.org/10.1093/bfgp/elm008

Beutner, D., Voets, T., Neher, E., & Moser, T. (2001). Calcium dependence of exocytosis and endocytosis at the cochlear inner hair cell afferent synapse. *Neuron*, 29, 681–690. https://doi.org/10.1016/S0896-6273(01)00243-4

Bloodgood, B. L., & Sabatini, B. L. (2007). Nonlinear regulation of unitary synaptic signals by $Ca_v2.3$ voltage-sensitive calcium channels located in dendritic spines. *Neuron*, 53, 249–260. https://doi.org/10.1016/j.neuron.2006.12.017

Bloodgood, B. L., & Sabatini, B. L. (2009). NMDA receptor-mediated calcium transients in dendritic spines. In A. M. Van Dongen (Ed.),

Biology of the NMDA receptor. Boca Raton, FL: CRC Press/Taylor & Francis.

Bogaerts, S., Clements, J. D., Sullivan, J. M., & Oleskevich, S. (2009). Automated threshold detection for auditory brainstem responses: Comparison with visual estimation in a stem cell transplantation study. *BMC Neuroscience*, *10*, 104. https://doi.org/10.1186/1471-2202-10-104

Brandt, A., Striessnig, J., & Moser, T. (2003). Ca$_v$1.3 channels are essential for development and presynaptic activity of cochlear inner hair cells. *Journal of Neuroscience*, *23*, 10832–10840.

Burkard, R. F., Eggermont, J. J., & Manuel, D. (Eds.) (2007). *Auditory evoked potentials: basic principles and clinical application.* Philadelphia: Lippincott Williams & Wilkins.

Catterall, W. A., Perez-Reyes, E., Snutch, T. P., & Striessnig, J. (2005). International Union of Pharmacology. XLVIII. Nomenclature and structure-function relationships of voltage-gated calcium channels. *Pharmacological Reviews*, *57*, 411–425.

Chen, S., Ren, Y. Q., Bing, R., & Hillman, D. E. (2000). Alpha 1E subunit of the R-type calcium channel is associated with myelinogenesis. *Journal of Neurocytology*, *29*, 719–728.

Chen, W. C., Xue, H. Z., Hsu, Y. L., Liu, Q., Patel, S., & Davis, R. L. (2011). Complex distribution patterns of voltage-gated calcium channel alpha-subunits in the spiral ganglion. *Hearing Research*, *278*, 52–68.

Dietrich, D., Kirschstein, T., Kukley, M., Pereverzev, A., von der Brelie, C., Schneider, T., & Beck, H. (2003). Functional specialization of presynaptic Ca$_v$2.3 Ca^{2+} channels. *Neuron*, *39*, 483–496. https://doi.org/10.1016/S0896-6273(03)00430-6

Dou, H., Vazquez, A. E., Namkung, Y., Chu, H., Cardell, E. L., Nie, L., … Yamoah, E. N. (2004). Null mutation of alpha1D Ca^{2+} channel gene results in deafness but no vestibular defect in mice. *Journal of the Association for Research in Otolaryngology*, *5*, 215–226.

Du, P., Kibbe, W. A., & Lin, S. M. (2006). Improved peak detection in mass spectrum by incorporating continuous wavelet transform-based pattern matching. *Bioinformatics*, *22*, 2059–2065. https://doi.org/10.1093/bioinformatics/btl355

Engel, J., Michna, M., Platzer, J., & Striessnig, J. (2002). Calcium channels in mouse hair cells: Function, properties and pharmacology. *Advances in Oto-Rhino-Laryngology*, *59*, 35–41.

Fell, B., Eckrich, S., Blum, K., Eckrich, T., Hecker, D., Obermair, G. J., … Engel, J. (2016). alpha2delta2 controls the function and trans-synaptic coupling of Ca$_v$1.3 channels in mouse inner hair cells and is essential for normal hearing. *Journal of Neuroscience*, *36*, 11024–11036.

Frank, T., Khimich, D., Neef, A., & Moser, T. (2009). Mechanisms contributing to synaptic Ca^{2+} signals and their heterogeneity in hair cells. *Proceedings of the National Academy of Sciences of the United States of America*, *106*, 4483–4488.

Galetin, T., Tevoufouet, E. E., Sandmeyer, J., Matthes, J., Nguemo, F., Hescheler, J., … Schneider, T. (2013). Pharmacoresistant Ca$_v$2.3 (E-type/R-type) voltage-gated calcium channels influence heart rate dynamics and may contribute to cardiac impulse conduction. *Cell Biochemistry and Function*, *31*, 434–449.

Gasparini, S., Kasyanov, A. M., Pietrobon, D., Voronin, L. L., & Cherubini, E. (2001). Presynaptic R-type calcium channels contribute to fast excitatory synaptic transmission in the rat hippocampus. *Journal of Neuroscience*, *21*, 8715–8721. https://doi.org/10.1523/JNEUROSCI.21-22-08715.2001

Glueckert, R., Wietzorrek, G., Kammen-Jolly, K., Scholtz, A., Stephan, K., Striessnig, J., & Schrott-Fischer, A. (2003). Role of class D L-type Ca^{2+} channels for cochlear morphology. *Hearing Research*, *178*, 95–105.

Goutman, J. D., & Glowatzki, E. (2007). Time course and calcium dependence of transmitter release at a single ribbon synapse. *Proceedings of the National Academy of Sciences of the United States of America*, *104*, 16341–16346.

Gu, Z., Steinmetz, L. M., Gu, X., Scharfe, C., Davis, R. W., & Li, W. H. (2003). Role of duplicate genes in genetic robustness against null mutations. *Nature*, *421*, 63–66. https://doi.org/10.1038/nature01198

Hellemans, J., Mortier, G., De Paepe, A., Speleman, F., & Vandesompele, J. (2007). qBase relative quantification framework and software for management and automated analysis of real-time quantitative PCR data. *Genome Biology*, *8*, R19.

Henry, K. R. (2004). Males lose hearing earlier in mouse models of late-onset age-related hearing loss; females lose hearing earlier in mouse models of early-onset hearing loss. *Hearing Research*, *190*, 141–148. https://doi.org/10.1016/S0378-5955(03)00401-5

Higley, M. J., & Sabatini, B. L. (2008). Calcium signaling in dendrites and spines: Practical and functional considerations. *Neuron*, *59*, 902–913. https://doi.org/10.1016/j.neuron.2008.08.020

Higley, M. J., & Sabatini, B. L. (2012). Calcium signaling in dendritic spines. *Cold Spring Harbor Perspectives in Biology 4*, a005686. https://doi.org/10.1101/cshperspect.a005686

Inagaki, A., & Lee, A. (2013). Developmental alterations in the biophysical properties of Ca$_v$1.3 Ca^{2+} channels in mouse inner hair cells. *Channels*, *7*, 171–181.

Inagaki, A., Ugawa, S., Yamamura, H., Murakami, S., & Shimada, S. (2008). The Ca$_v$3.1 T-type Ca^{2+} channel contributes to voltage-dependent calcium currents in rat outer hair cells. *Brain Research*, *1201*, 68–77. https://doi.org/10.1016/j.brainres.2008.01.058

Ison, J. R., Allen, P. D., & O'Neill, W. E. (2007). Age-related hearing loss in C57BL/6J mice has both frequency-specific and non-frequency-specific components that produce a hyperacusis-like exaggeration of the acoustic startle reflex. *Journal of the Association for Research in Otolaryngology*, *8*, 539–550. https://doi.org/10.1007/s10162-007-0098-3

Johnson, S. L., & Marcotti, W. (2008). Biophysical properties of Ca$_v$1.3 calcium channels in gerbil inner hair cells. *Journal of Physiology*, *586*, 1029–1042.

Johnson, S. L., Marcotti, W., & Kros, C. J. (2005). Increase in efficiency and reduction in Ca^{2+} dependence of exocytosis during development of mouse inner hair cells. *Journal of Physiology*, *563*, 177–191.

Joiner, M. L., & Lee, A. (2015). Voltage-gated Ca$_v$1 channels in disorders of vision and hearing. *Current Molecular Pharmacology*, *8*, 143–148.

Jurkovicova-Tarabova, B., Griesemer, D., Pirone, A., Sinnegger-Brauns, M. J., Striessnig, J., & Friauf, E. (2012). Repertoire of high voltage-activated Ca^{2+} channels in the lateral superior olive: Functional analysis in wild-type, Ca$_v$1.3$^{-/-}$, and Ca$_v$1.2DHP$^{-/-}$ mice. *Journal of Neurophysiology*, *108*, 365–379.

Kallstrand, J., Lewander, T., Baghdassarian, E., & Nielzen, S. (2014). A new method for analyzing auditory brain-stem response waveforms using a moving-minimum subtraction procedure of digitized analog recordings. *Neuropsychiatric Disease and Treatment*, *10*, 1011–1016.

Kang, H. W., Park, J. Y., Jeong, S. W., Kim, J. A., Moon, H. J., Perez-Reyes, E., & Lee, J. H. (2006). A molecular determinant of nickel inhibition in Ca$_v$3.2 T-type calcium channels. *Journal of Biological Chemistry*, *281*, 4823–4830.

Kim, M. H., Li, G. L., & von Gersdorff, G. H. (2013). Single Ca^{2+} channels and exocytosis at sensory synapses. *Journal of Physiology*, *591*, 3167–3178.

Kim, Y., & Trussell, L. O. (2007). Ion channels generating complex spikes in cartwheel cells of the dorsal cochlear nucleus. *Journal of Neurophysiology*, *97*, 1705–1725. https://doi.org/10.1152/jn.00536.2006

Knipper, M., Van Dijk, P., Nunes, I., Ruttiger, L., & Zimmermann, U. (2013). Advances in the neurobiology of hearing disorders: Recent developments regarding the basis of tinnitus and hyperacusis. *Progress in Neurobiology*, *111*, 17–33. https://doi.org/10.1016/j.pneurobio.2013.08.002

Koschak, A., Reimer, D., Huber, I., Grabner, M., Glossmann, H., Engel, J., & Striessnig, J. (2001). alpha 1D (Ca_v1.3) subunits can form l-type Ca^{2+} channels activating at negative voltages. *Journal of Biological Chemistry*, *276*, 22100–22106.

Kuzmiski, J. B., Barr, W., Zamponi, G. W., & MacVicar, B. A. (2005). Topiramate inhibits the initiation of plateau potentials in CA1 neurons by depressing R-type calcium channels. *Epilepsia*, *46*, 481–489. https://doi.org/10.1111/j.0013-9580.2005.35304.x

Layton, M. G., Robertson, D., Everett, A. W., Mulders, W. H., & Yates, G. K. (2005). Cellular localization of voltage-gated calcium channels and synaptic vesicle-associated proteins in the guinea pig cochlea. *Journal of Molecular Neuroscience*, *27*, 225–244. https://doi.org/10.1385/JMN:27:2:225

Lei, D., Gao, X., Perez, P., Ohlemiller, K. K., Chen, C. C., Campbell, K. P., … Bao, J. (2011). Anti-epileptic drugs delay age-related loss of spiral ganglion neurons via T-type calcium channel. *Hearing Research*, *278*, 106–112.

Lu, Z. J., Pereverzev, A., Liu, H. L., Weiergraber, M., Henry, M., Krieger, A., … Schneider, T. (2004). Arrhythmia in isolated prenatal hearts after ablation of the Ca_v2.3 (alpha1E) subunit of voltage-gated Ca^{2+} channels. *Cellular Physiology and Biochemistry*, *14*, 11–22.

Lundt, A., Seidel, R., Soos, J., Henseler, C., Muller, R., Bakki, M., … Weiergraber, M. (2019). Ca_v3.2 T-type calcium channels are physiologically mandatory for the auditory system. *Neuroscience*, *409*, 81–100. https://doi.org/10.1016/j.neuroscience.2019.04.024

Lundt, A., Soos, J., Henseler, C., Arshaad, M. I., Müller, R., Ehninger, D., … Weiergräber, M. (2019) Data acquisition and analysis in brainstem evoked response audiometry in mice. *Journal of Visualized Experiments*, *147*, 1–12.

Lv, P., Sihn, C. R., Wang, W., Shen, H., Kim, H. J., Rocha-Sanchez, S. M., & Yamoah, E. N. (2012). Posthearing Ca^{2+} currents and their roles in shaping the different modes of firing of spiral ganglion neurons. *Journal of Neuroscience*, *32*, 16314–16330. https://doi.org/10.1523/JNEUROSCI.2097-12.2012

Marcotti, W., Johnson, S. L., Holley, M. C., & Kros, C. J. (2003). Developmental changes in the expression of potassium currents of embryonic, neonatal and mature mouse inner hair cells. *Journal of Physiology*, *548*, 383–400. https://doi.org/10.1113/jphysiol.2002.034801

Martini, M., Rossi, M. L., Rubbini, G., & Rispoli, G. (2000). Calcium currents in hair cells isolated from semicircular canals of the frog. *Biophysical Journal*, *78*, 1240–1254.

Matthews, E. A., Bee, L. A., Stephens, G. J., & Dickenson, A. H. (2007). The Ca_v2.3 calcium channel antagonist SNX-482 reduces dorsal horn neuronal responses in a rat model of chronic neuropathic pain. *European Journal of Neuroscience*, *25*, 3561–3569.

Michna, M., Knirsch, M., Hoda, J. C., Muenkner, S., Langer, P., Platzer, J., … Engel, J. (2003). Ca_v1.3 (alpha1D) Ca^{2+} currents in neonatal outer hair cells of mice. *Journal of Physiology*, *553*, 747–758.

Moser, T., & Beutner, D. (2000). Kinetics of exocytosis and endocytosis at the cochlear inner hair cell afferent synapse of the mouse. *Proceedings of the National Academy of Sciences of the United States of America*, *97*, 883–888.

Muller, R., Struck, H., Ho, M. S., Brockhaus-Dumke, A., Klosterkotter, J., Broich, K., … Weiergraber, M. (2012). Atropine-sensitive hippocampal theta oscillations are mediated by Ca_v2.3 R-type Ca^{2+} channels. *Neuroscience*, *205*, 125–139. https://doi.org/10.1016/j.neuroscience.2011.12.032

Murphy, M. P., & Gates, G. A. (1997). Hearing loss: Does gender play a role? *Medscape Womens Health*, *2*, 2.

Nemzou, N. R., Bulankina, A. V., Khimich, D., Giese, A., & Moser, T. (2006). Synaptic organization in cochlear inner hair cells deficient for the Ca_v1.3 (alpha1D) subunit of L-type Ca^{2+} channels. *Neuroscience*, *141*, 1849–1860.

Nie, L., Zhu, J., Gratton, M. A., Liao, A., Mu, K. J., Nonner, W., … Yamoah, E. N. (2008). Molecular identity and functional properties of a novel T-type Ca^{2+} channel cloned from the sensory epithelia of the mouse inner ear. *Journal of Neurophysiology*, *100*, 2287–2299.

Pangrsic, T., Singer, J. H., & Koschak, A. (2018). Voltage-gated calcium channels: Key players in sensory coding in the retina and the inner ear. *Physiological Reviews*, *98*, 2063–2096. https://doi.org/10.1152/physrev.00030.2017

Parajuli, L. K., Nakajima, C., Kulik, A., Matsui, K., Schneider, T., Shigemoto, R., & Fukazawa, Y. (2012). Quantitative regional and ultrastructural localization of the Ca_v2.3 subunit of R-type calcium channel in mouse brain. *Journal of Neuroscience*, *32*, 13555–13567. https://doi.org/10.1523/JNEUROSCI.1142-12.2012

Pearson, J. D., Morrell, C. H., Gordon-Salant, S., Brant, L. J., Metter, E. J., Klein, L. L., & Fozard, J. L. (1995). Gender differences in a longitudinal study of age-associated hearing loss. *Journal of the Acoustical Society of America*, *97*, 1196–1205. https://doi.org/10.1121/1.412231

Peng, H., Xie, D. H., Xiao, Z. A., Wu, W. J., Chen, Y., & Xia, K. (2004). [Subunit of voltage-dependent calcium channels in the murine spiral ganglion cells]. *Zhonghua Er Bi Yan Hou Ke Za Zhi*, *39*, 385–388.

Pereverzev, A., Mikhna, M., Vajna, R., Gissel, C., Henry, M., Weiergraber, M., … Schneider, T. (2002). Disturbances in glucose-tolerance, insulin-release, and stress-induced hyperglycemia upon disruption of the Ca_v2.3 (alpha 1E) subunit of voltage-gated Ca^{2+} channels. *Molecular Endocrinology*, *16*, 884–895.

Perez-Reyes, E. (2003). Molecular physiology of low-voltage-activated T-type calcium channels. *Physiological Reviews*, *83*, 117–161. https://doi.org/10.1152/physrev.00018.2002

Picher, M. M., Gehrt, A., Meese, S., Ivanovic, A., Predoehl, F., Jung, S., … Moser, T. (2017). Ca^{2+}-binding protein 2 inhibits Ca^{2+}-channel inactivation in mouse inner hair cells. *Proceedings of the National Academy of Sciences of the United States of America*, *114*, E1717–E1726.

Platzer, J., Engel, J., Schrott-Fischer, A., Stephan, K., Bova, S., Chen, H., … Striessnig, J. (2000). Congenital deafness and sinoatrial node dysfunction in mice lacking class D L-type Ca^{2+} channels. *Cell*, *102*, 89–97. https://doi.org/10.1016/S0092-8674(00)00013-1

Probst, F. J., Corrigan, R. R., Del Gaudio, D., Salinger, A. P., Lorenzo, I., Gao, S. S., … Justice, M. J. (2013). A point mutation in the gene

for asparagine-linked glycosylation 10B (Alg10b) causes nonsyndromic hearing impairment in mice (Mus musculus). *PLoS ONE*, *8*, e80408. https://doi.org/10.1371/journal.pone.0080408

Rodriguez-Contreras, A., & Yamoah, E. N. (2001). Direct measurement of single-channel Ca^{2+} currents in bullfrog hair cells reveals two distinct channel subtypes. *The Journal of Physiology.*, *534*, 669–689.

Shcheglovitov, A., Vitko, I., Lazarenko, R. M., Orestes, P., Todorovic, S. M., & Perez-Reyes, E. (2012). Molecular and biophysical basis of glutamate and trace metal modulation of voltage-gated $Ca_v2.3$ calcium channels. *Journal of General Physiology*, *139*, 219–234.

Sheets, L., Kindt, K. S., & Nicolson, T. (2012). Presynaptic Ca 1.3 channels regulate synaptic ribbon size and are required for synaptic maintenance in sensory hair cells. *The Journal of Neuroscience*, *32*, 17273–17286. https://doi.org/10.1523/JNEUROSCI.3005-12.2012

Shen, H., Zhang, B., Shin, J. H., Lei, D., Du, Y., Gao, X., … Bao, J. (2007). Prophylactic and therapeutic functions of T-type calcium blockers against noise-induced hearing loss. *Hearing Research*, *226*, 52–60.

Siwek, M. E., Muller, R., Henseler, C., Broich, K., Papazoglou, A., & Weiergraber, M. (2014). The $Ca_v2.3$ R-type voltage-gated Ca^{2+} channel in mouse sleep architecture. *Sleep*, *37*, 881–892. https://doi.org/10.5665/sleep.3652

Soong, T. W., Stea, A., Hodson, C. D., Dubel, S. J., Vincent, S. R., & Snutch, T. P. (1993). Structure and functional expression of a member of the low voltage-activated calcium channel family. *Science*, *260*, 1133–1136. https://doi.org/10.1126/science.8388125

Spassova, M., Eisen, M. D., Saunders, J. C., & Parsons, T. D. (2001). Chick cochlear hair cell exocytosis mediated by dihydropyridine-sensitive calcium channels. *The Journal of Physiology*, *535*, 689–696.

Stephens, G. J., Page, K. M., Burley, J. R., Berrow, N. S., & Dolphin, A. C. (1997). Functional expression of rat brain cloned alpha1E calcium channels in COS-7 cells. *Pflugers Archiv*, *433*, 523–532.

Su, Z. L., Jiang, S. C., Gu, R., & Yang, W. P. (1995). Two types of calcium channels in bullfrog saccular hair cells. *Hearing Research*, *87*, 62–68.

Suzuki, T., Delgado-Escueta, A. V., Aguan, K., Alonso, M. E., Shi, J., Hara, Y., … Yamakawa, K. (2004). Mutations in EFHC1 cause juvenile myoclonic epilepsy. *Nature Genetics*, *36*, 842–849. https://doi.org/10.1038/ng1393

Tai, C., Kuzmiski, J. B., & MacVicar, B. A. (2006). Muscarinic enhancement of R-type calcium currents in hippocampal CA1 pyramidal neurons. *Journal of Neuroscience*, *26*, 6249–6258. https://doi.org/10.1523/JNEUROSCI.1009-06.2006

Thomas, J. H. (1993). Thinking about genetic redundancy. *Trends in Genetics*, *9*, 395–399. https://doi.org/10.1016/0168-9525(93)90140-D

Waka, N., Knipper, M., & Engel, J. (2003). Localization of the calcium channel subunits $Ca_v1.2$ (alpha1C) and $Ca_v2.3$ (alpha1E) in the mouse organ of Corti. *Histology and Histopathology*, *18*, 1115–1123.

Weiergraber, M., Henry, M., Krieger, A., Kamp, M., Radhakrishnan, K., Hescheler, J., & Schneider, T. (2006a). Altered seizure susceptibility in mice lacking the $Ca_v2.3$ E-type Ca^{2+} channel. *Epilepsia*, *47*, 839–850. https://doi.org/10.1111/j.1528-1167.2006.00541.x

Weiergraber, M., Henry, M., Radhakrishnan, K., Hescheler, J., & Schneider, T. (2007). Hippocampal seizure resistance and reduced neuronal excitotoxicity in mice lacking the $Ca_v2.3$ E/R-type voltage-gated calcium channel. *Journal of Neurophysiology*, *97*, 3660–3669.

Weiergraber, M., Henry, M., Sudkamp, M., de Vivie, E. R., Hescheler, J., & Schneider, T. (2005). Ablation of $Ca_v2.3$ / E-type voltage-gated calcium channel results in cardiac arrhythmia and altered autonomic control within the murine cardiovascular system. *Basic Research in Cardiology*, *100*, 1–13.

Weiergraber, M., Kamp, M. A., Radhakrishnan, K., Hescheler, J., & Schneider, T. (2006b). The Cav2.3 voltage-gated calcium channel in epileptogenesis–shedding new light on an enigmatic channel. *Neuroscience and Biobehavioral Reviews*, *30*, 1122–1144. https://doi.org/10.1016/j.neubiorev.2006.07.004

Weiergraber, M., Stephani, U., & Kohling, R. (2010). Voltage-gated calcium channels in the etiopathogenesis and treatment of absence epilepsy. *Brain Research Reviews*, *62*, 245–271.

Williams, M. E., Marubio, L. M., Deal, C. R., Hans, M., Brust, P. F., Philipson, L. H., … Ellis, S. B. (1994). Structure and functional characterization of neuronal alpha 1E calcium channel subtypes. *Journal of Biological Chemistry*, *269*, 22347–22357.

Wilson, S. M., Toth, P. T., Oh, S. B., Gillard, S. E., Volsen, S., Ren, D., … Miller, R. J. (2000). The status of voltage-dependent calcium channels in alpha 1E knock-out mice. *Journal of Neuroscience*, *20*, 8566–8571.

Wu, L. G., Westenbroek, R. E., Borst, J. G., Catterall, W. A., & Sakmann, B. (1999). Calcium channel types with distinct presynaptic localization couple differentially to transmitter release in single calyx-type synapses. *Journal of Neuroscience*, *19*, 726–736. https://doi.org/10.1523/JNEUROSCI.19-02-00726.1999

Xu, W., & Lipscombe, D. (2001). Neuronal $Ca_v1.3$ alpha1 L-type channels activate at relatively hyperpolarized membrane potentials and are incompletely inhibited by dihydropyridines. *Journal of Neuroscience*, *21*, 5944–5951.

Yang, S. N., & Berggren, P. O. (2005). Beta-cell Ca_v channel regulation in physiology and pathophysiology. *American Journal of Physiology Endocrinology and Metabolism*, *288*, E16–E28.

Yasuda, R., Sabatini, B. L., & Svoboda, K. (2003). Plasticity of calcium channels in dendritic spines. *Nature Neuroscience*, *6*, 948–955. https://doi.org/10.1038/nn1112

Yokoyama, C. T., Westenbroek, R. E., Hell, J. W., Soong, T. W., Snutch, T. P., & Catterall, W. A. (1995). Biochemical properties and subcellular distribution of the neuronal class E calcium channel alpha 1 subunit. *Journal of Neuroscience*, *15*, 6419–6432. https://doi.org/10.1523/JNEUROSCI.15-10-06419.1995

Yokoyama, K., Kurihara, T., Saegusa, H., Zong, S., Makita, K., & Tanabe, T. (2004). Blocking the R-type ($Ca_v2.3$) Ca^{2+} channel enhanced morphine analgesia and reduced morphine tolerance. *European Journal of Neuroscience*, *20*, 3516–3519. https://doi.org/10.1111/j.1460-9568.2004.03810.x

Zaman, T., Lee, K., Park, C., Paydar, A., Choi, J. H., Cheong, E., … Shin, H. S. (2011). $Ca_v2.3$ channels are critical for oscillatory burst discharges in the reticular thalamus and absence epilepsy. *Neuron*, *70*, 95–108. https://doi.org/10.1016/j.neuron.2011.02.042

Zampini, V., Johnson, S. L., Franz, C., Knipper, M., Holley, M. C., Magistretti, J., … Marcotti, W. (2013). Burst activity and ultrafast activation kinetics of $Ca_v1.3$ Ca^{2+} channels support presynaptic activity in adult gerbil hair cell ribbon synapses. *Journal of Physiology*, *591*, 3811–3820.

Zampini, V., Johnson, S. L., Franz, C., Lawrence, N. D., Munkner, S., Engel, J., … Marcotti, W. (2010). Elementary properties of $Ca_v1.3$ Ca^{2+} channels expressed in mouse cochlear inner hair cells. *Journal of Physiology*, *588*, 187–199.

Zorrilla de San, M. J., Pyott, S., Ballestero, J., & Katz, E. (2010). Ca^{2+} and Ca^{2+}-activated K^+ channels that support and modulate transmitter release at the olivocochlear efferent-inner hair cell synapse. *Journal of Neuroscience*, *30*, 12157–12167. https://doi.org/10.1523/JNEUROSCI.2541-10.2010

SUPPORTING INFORMATION

Additional supporting information may be found online in the Supporting Information section.